CMTLIN REFERENCE NUMBER

AED-Conf-63-048-126

[illegible] PARTICLES PRODUCED IN NUCLEAR [illegible] AT ~ 10^{12} eV

C. O. Kim

American Physical Society
1963 Spring Meeting
Washington, D. C.
April 22-25, 1963

conf-630422

46-117

Kim, C. O.

DISCLAIMER

EFINS 64-12

COMPOSITION OF THE SECONDARY PARTICLES PRODUCED IN NUCLEAR INTERACTION AT ~ 10^{12} eV

C. O. Kim

The Department of Physics and
The Enrico Fermi Institute for Nuclear Studies
The University of Chicago
Chicago, Illinois

Submitted to the Physical Review

February, 1964

TABLE OF CONTENTS

Composition of the Secondary Particles Produced in Nuclear Interaction at ~10^{12} eV*†

C. O. Kim

The Enrico Fermi Institute for Nuclear Studies
and
The Department of Physics
The University of Chicago
Chicago, Illinois

ABSTRACT

Twenty-two proton, neutron, and alpha jets ($N_h \leq 3$, 2×10^{11} eV $< E < 1.5 \times 10^{13}$ eV) found in a 22-liter emulsion stack flown for 13 hours at an altitude of 116,000 feet, have been analyzed to identify the nature of the particles emitted in the extreme backward c.m. cone. Among 82 tracks analyzed, out of 149 tracks traced (total length of the secondaries traced was 20.4 m, and 74 interactions were found), 53 secondaries were attributed to pions, 18 to kaons, 10 to protons, and one to a hyperon. The relative composition of the 82 secondaries has a dependence on the c.m. emission angle $\bar{\theta}$. For $\bar{\theta} \geq 175^\circ$, there were 7 π, 9 K, 10 p, and 1 Y; for $\bar{\theta} < 175^\circ$, there were 46 π, 9 K, and no baryons. Similar distinction existed for the

---

*Research supported by the National Science Foundation and the United States Office of Naval Research.

†This paper is based on a thesis submitted to the Department of Physics, the University of Chicago, in partial fulfillment of the requirements for the Ph.D. degree (August, 1963). Preliminary reports of this work were given in Bull. Am. Phys. Soc. II, 8, 293 (1963) and in the Proceedings of the International Conference on Cosmic Rays at Jaipur, India (December, 1963).

average c.m. momenta $\langle\bar{p}\rangle$ and the average transverse momenta $\langle p_t\rangle$ as follows:

	$\langle\bar{p}\rangle$ (GeV/c)			$\langle p_t\rangle$ (GeV/c)		
	π	K	p	π	K	p
$\bar{\theta} \geq 175^\circ$	8.5	14.3	26	.20 ± .08	.21 ± .07	.35 ± .11
$\bar{\theta} < 175^\circ$	1.1	1.5	-	.32 ± .05	.46 ± .15	
Overall	2.1	7.9	26	.31	.33	.35

The baryons carried the average fraction .5 ± .2 of the total available energy in the c.m. system. Concerning the K/π ratio, p_t distribution, and $\langle\bar{p}\rangle$ at $\bar{\theta} < 175^\circ$, the hydrodynamical theory with a critical temperature $kT_c \cong m_\pi c^2$ predicts the correct behavior. In this region, the c.m. momentum distribution of pions is of the form $dN \propto \bar{p}^n\, d\bar{p}$ with $n = -.9 \pm .4$. But for $\bar{\theta} \geq 175^\circ$, the smallness of $\langle p_t\rangle$ favors an interpretation in terms of the Heisenberg theory, since this theory predicts $p_t \approx m_\pi c$ and high K/π ratio in the extreme backward and forward c.m. emission angle region.

I. INTRODUCTION

In the very high-energy nuclear interactions, a large fraction of the created particles are narrowly collimated in the direction of the primary incoming particles as a consequence of the great velocity of the c.m. system of the incident and target particles. These events, which are produced by high-energy cosmic rays and recorded mostly by means of big emulsion stacks flown by balloons at the top of the atmosphere, are known as "jets". There are excellent review articles available on the subject.[1,2] It is well established that the created particles (secondaries) are composed mostly of pions. The exact relative frequencies of occurrence of pions, kaons, nucleons, and hyperons are, however, not well known. At accelerator energies up to ~ 30 GeV, this problem has been investigated fairly well,[3,4] and the question is open whether such frequencies remain constant at higher energies.

Two <u>indirect</u> methods have been used to investigate this problem.[1,2] A first approach consists in the measurement of the frequency of electron pairs versus that of charged secondaries in the core of jets. Since electron pairs are assumed to arise from the materialization of decay γ rays of neutral pions, the frequency of these electron pairs gives an estimate of the production rate of neutral pions. The number of created charged pions is then inferred, equal to twice the number of neutral pions, since charge independence is expected to hold in the production process, provided the pions are produced directly. Then the number of charged secondaries

subtracted from that inferred for charged pions in a given solid angle will give the portion of non-pionic charged secondaries. A second estimate is obtained from the observation of the frequency of secondary nuclear interactions produced by neutral particles, which are definitely non-pionic in origin. Both methods give an estimate of ~ 20% for the frequency of non-pionic secondaries at energies above 10^{12} eV.

The direct approach to this problem is concerned with the identification of the secondaries emitted backward in the c.m. system of the two colliding nucleons, with respect to the direction of the incident particle. In fact, the masses of such secondaries can be often established by measurements of grain density, scattering, and range when they emerge in the laboratory system with energies $\lesssim$ 10 GeV.[5,6] On the other hand, the forward-emitted secondaries are too energetic in the laboratory system for identification by conventional methods. However, several plausible models of a single nucleon-nucleon collision suggest that the secondaries in the backward and forward cones must possess, on the average, overall symmetry with respect to the center of mass, as to both composition and angular distribution. Brisbout et al.[7] further attempted to estimate the non-pionic portion of secondaries from an analysis of the tertiary products emerging from the interactions of the backward-cone secondaries. In their study the tracks of secondaries were followed for 17 meters and 51 interactions were observed, 32 of which were studied; one kaon and one hyperon were observed among the tertiary particles. One unstable secondary was also reported.

The present investigation follows the above authors' approach. The energy of the jets studied here is in the range of 2×10^{11} eV to 1.5×10^{13} eV. An attempt has been made to identify 149 secondaries belonging to the c.m. backward cone. The large volume of the stack employed here (22 liter) was used to full advantage. Not only multiple scattering and ionization measurements could be performed on very long tracks, but in several cases the variation of ionization along the path of the secondaries could be detected. In this way 82 of the secondaries studied could be identified.

Finally, several important features of high-energy nucleon-nucleon collisions are investigated here, such as the longitudinal and transverse momentum distributions of the secondaries in the c.m. system and the dependence of these quantities on emission angles and particle composition.

II. EXPERIMENTAL MATERIAL

1. Properties of the Emulsion Stack

A 22 liter stack of Ilford G-5 emulsion, consisting of [illegible]

at an altitude of 116,000 feet for thirteen hours, was used for the present experiment. Many investigations on various aspects of high-energy phenomena based on the material contained in this stack were previously reported.[8-15] Data referring to the flight curve, the construction of the stack and scanning procedures are contained particularly in Refs. 8 and 10.

Several details, pertinent to the present investigation,

should, however, be mentioned here. The stack was processed in batches of 36 plates per day by the "dry" method of Bonetti et al.[16] Three months elapsed between exposure and development, while the new Ryerson processing plant was built.

The mean grain densities, g_o, of high-energy electrons are shown in Fig. 1. The mean grain densities, g_o, remain reasonably constant for the group of plates No. 1 - No. 112, which were processed last. The fluctuation of grain density for the rest of the plates can be attributed to the setting-up of the routine in the new processing plant. The tracks of high-energy electrons were carefully selected from the electromagnetic showers and were estimated to have energies $\simeq$ 100 MeV, or within ~ 2% of the relativistic plateau of grain density. The depth dependence of grain density, $g_o(z)$, of the high-energy electrons, on the depth, z, measured from the glass surface of the emulsion was constructed for several plates and was tested using the very high-energy electron pairs in the cores of jets. Figure 2 shows the typical dependence of the grain density, $g_o(z)$, which is normalized by g_o of the plate where $g_o = \int g_o(z)\, dz$. In spite of the large variation with the depth the mean grain density, g_o, was consistently the same over different regions for each plate.

The one-millimeter LRL grid[17] was photographically printed on the glass side of the emulsion and these coordinate readings were used for the range measurements and for aid in tracing. The alignment of the grid from a plate to the next was well within 1/2 mm. The grid system and the "landmarks"

provided by local tracks enabled about 10,000 traversals of shower particles and tertiary particles between plates with about 26 impossible cases, which resulted mostly from crossing the cut edges which became rugged after cutting.

The stack had two shortcomings: (i) No systematic measurements of thickness of the emulsion prior to development were made. (ii) The density of the emulsion during the flight is not known. Thus, all the plates in the stack were assumed to be exactly 600 μm before processing and of the standard density, 3.815 gm/cm^2. The results of the present experiment, however, mostly based on measurements of multiple Coulomb scatterings and ionization, are particularly insensitive to variation in such parameters, at least within the limits known for typical emulsion stacks.

2. Scanning

Each plate of this stack was scanned with 22X oil objectives and 12.5X oculars for groups of parallel and minimum-ionizing tracks along scanning lines defining 15 cm x 15 cm squares. From about 2,000 groups of associated shower tracks that were found on the scanning lines, all showers having more than ten parallel tracks in one field of view were traced back to their origin.[10] The scanning criterion corresponds to a lower limit of about 100 GeV for the energy contained in the electron-photon component of the showers. A total of 120 nuclear interactions (78 p, 6 n, 27 α, and 9 H) were found. Among 84 p or n events, 57 events with dip angles less than 17° were analyzed and reported by Barkow *et al.*[8] Jain[9]

reported the results of the analysis of 17 α jets with dip angles less than 20°.

3. Selection of Jets and of Tracks for Analysis

Among these nuclear interactions, 22 jets of proton, α, or neutral primaries, which satisfied the following criteria, were chosen for the present study:

(i) The primary had a track length of more than 2 mm per plate.

(ii) The potential length of the jet axis in the stack was larger than 20 cm.

(iii) The number of grey or heavy tracks, $N_h \leq 3$.

(iv) The estimated energy was greater than 10^{11} eV.

Condition (i) was imposed to ensure having secondaries of favorable geometry, condition (ii) gives the secondaries more chances to interact in the detector, condition (iii) selects either primaries' collision with hydrogen or with emulsion nuclei in which the effect of collisions with more than one nucleon is minimal. The relevant data for these events are listed in Table I. Indicated are the event number, the type of jet in accordance with the standard nomenclature (n_s corresponds to the number of secondaries with the normalized grain density $g^* < 1.5$), the Castagnoli energy E_{cast},[18] the energy carried by the charged secondaries defined as $E_{ch} = [\Sigma .4 \text{ GeV}/\sin \theta_i]$ by assuming the transverse momenta of the secondaries as .4 GeV/c and constant, the track length of primaries per plate, the spread of the distribution

$$\sigma = [\Sigma(\log \tan \theta_i - \langle \log \tan \theta_i \rangle)^2/(n_s - 1)]^{1/2},$$

and the potential length of the jet axis in the stack. The emission angles θ_i refer to the centroid of the secondaries in the laboratory system. For most p and n events E_{cast} and the particle multiplicities correspond to those given in Ref. 8. Only for event No. 63 a new energy estimate is given here. E_{ch} was calculated from the plot of log tan θ_i in Ref. 8. The seven α events were thoroughly reanalyzed. In all cases the emission angles of the backward-cone secondaries were carefully remeasured with respect to the direction of the incident primary. The plots of log tan θ_i for the 22 events, inclusive of small corrections from the remeasurements, are shown in Figs. 3 (a) and (b).

Out of 501 shower particle tracks, the following were selected for measurement:

(i) All those belonging to 1/8 of the charged secondaries in the extreme backward-cone. Such tracks were traced to their ends in the stack, regardless of dip angles. Four grey tracks with normalized grain density $1.5 < g^* \leq 3.2$, later identified as protons, were also included in this analysis.

(ii) All tracks of length ≥ 5 mm per plate, not included in (i), to cover about 1/4 of the charged secondaries in the extreme backward-cone. Such tracks were traced.

The composite angular distribution of the 22 jets is shown in Fig. 4. The solid line histogram refers to the tracks contained in 1/4 of the charged secondaries in the backward-cone, while

the shaded area represents the portion of secondaries which were actually traced. In addition, the grey and black prongs of all the primary interactions were also traced to their ends in the stack. When the secondaries being followed interacted, the numbers of black, grey, and shower particles in the secondary stars were carefully determined. Grey and black tertiary particles from all the secondary interactions were then in turn traced throughout the stack.

Table II summarizes the results of tracing secondaries. A total of 74 interactions was found in tracing 20.4 meters of secondaries. (The corresponding interaction mean free path is 27.2 cm in place of the geometrical mean free path in emulsion of 28 cm.) Twenty-six tracks out of 149 were lost in tracing. Only one of the four grey secondaries included in the analysis came to rest among all the secondaries analyzed and was identified as a 130 MeV proton.

III. IDENTIFICATION OF JET SECONDARIES

Aside from the rare occurrence of decays in flight or strangeness conserving interactions, the systematic identification of charged jet secondaries stems from the measurements of quantities depending on their electromagnetic interaction. Thus, the mass of a secondary was determined essentially with the following two standard methods, which were sometimes employed simultaneously:

a) The parameter m_i in the function $g^* = f[(R_i/m_i)]$, where g^* is the grain density of a secondary normalized to that for shower electrons, $g^* = g/g_o$, and R_i

the residual range, was determined by measuring the variation of the normalized grain density $\Delta g^* = g^*_2 - g^*_1$ at a value of g^*_1 over a distance, $\Delta R_i = R_{i2} - R_{i1}$. This was, of course, possible only if the thickness ΔR_i of emulsion traversed was large enough to moderate appreciably the energy of the secondary.

b) The mass m_i in $p\beta = m_i\gamma\beta^2$ was determined by combining the value of the $p\beta$, obtained from measurement of multiple Coulomb scatterings with that of the normalized grain density, g^*, which to a good approximation is a function only of the velocity, β, and not of the mass.

The function $g^* = f[(R_i/m_i)]$ could be established by measurements on known particles in the region of $\beta \lesssim .95$ (pre-minimum region), while $g^* = F(p\beta)$ beyond the minimum ionization (trans-minimum region) is essentially predicted on theoretical grounds; these functions were then used to attempt particle identification. The details of the grain density and scattering measurements are described in Appendix I.

1. Grain Density Calibration in the Pre-Minimum Region

The grain density in the region $.62 \leq \beta \leq .83$ was established using tracks of stopping π^+, identified by their characteristic π-μ-e decay. The pions were traced back from their decay point and counting was performed in the region of residual range from 2 to 12 cm. This calibration is shown in Fig. 5 where the solid curve is a best fit to the experimental points. The curves for kaons and protons were derived from the latter.

It was possible to extend the curve further down to the region of minimum ionization by observing the variations of g* for jet secondaries, even if they did not stop or decay in the stack. This is shown in Fig. 5 where the observed variation in the normalized grain density, over an interval ΔR, is fitted to extrapolate the curves obtained up to $\beta \approx .95$. By this procedure some of the secondaries were also identified. The region thus calibrated is indicated by dotted curves in Fig. 5. The same symbol is used to represent points of the same secondary.

2. The Theoretical Grain Density in the Relativistic Region

The average energy loss per unit path by ionization of a singly charged particle of velocity β in unit of the velocity of light c may be expressed by the modified Bethe-Block formula[19-21]

$$-\frac{dE}{dx} = \frac{2\pi n_e e^4}{mc^2\beta^2}\left(\ln \frac{2mc^2\beta^2\gamma^2 T}{\omega^2} - 2\beta^2 - \Delta\right) \qquad (1)$$

where

n_e = number of electrons per unit volume

m = electron mass

$\gamma = (1 - \beta^2)^{-1/2}$

ω = average ionization potential of atoms in the medium

T = maximum energy transfer to an electron; for a heavy particle of

$$T = \frac{(\gamma^2 - 1)m_i c^2}{m_i/2m + m/2m_i + \gamma}$$

Δ = the correction for the density effect.

But as stressed by many authors,[20, 22-24] the "restricted" rate

of energy loss, I_r, which is to be compared with grain density in emulsion, arises from absorption only in AgBr crystals along the track, and can be expressed as

$$I_r = \frac{2\pi n'_e e^4}{mc^2\beta^2}\left(\ln\frac{2mc^2\beta^2\gamma^2 T_o}{\omega'^2} - \beta^2 - \Delta'\right) \qquad (2)$$

where T_o is the maximum energy of delta-rays which are contained in the dimension of a single grain. The dashed quantities refer here to AgBr. The correction Δ' for the density effect, which is very critical for the present purpose, is approximated by the analytical expressions given by Sternheimer[25,26]

$$\begin{aligned} \Delta' &= \ln\beta^2\gamma^2 + C' + .0235\,(4 - x)^{4.03} && \text{for } .30 < x < 4 \\ \Delta' &= \ln\beta^2\gamma^2 + C' && \text{for } x \geq 4 \end{aligned} \qquad (3)$$

where

$$x = \log_{10}\beta\gamma;\quad C' = -\ln[\omega'^2/(h\nu'_p)^2] - 1;\quad \nu'_p = \sqrt{n'_e e^2/\pi m}$$

So I_r in Eq. (2) becomes

$$I_r = \frac{2\pi n'_e e^4}{mc^2\beta^2}\left[\ln\frac{2mc^2 T_o}{(h\nu'_p)^2} - \beta^2 + 1 - .0235\,(4 - x)^{4.03}\right] \qquad \text{for } .30 < x < 4$$

and the asymptotic plateau value $I_r(\beta = 1)$ becomes

$$I_r(\beta = 1) = \frac{2\pi n'_e e^4}{mc^2}\ln\frac{2mc^2 T_o}{(h\nu'_p)^2} \qquad (4)$$

where there is no longer a dependence on the ionization potential as such, but only on the electron density n'_e in the medium linearly and through the plasma frequency ν'_p. Then the theoretical expression $g^{**} = I_r/I_r(\beta = 1)$, which is to be compared with the normalized grain density g^*, is given as

$$g^{**} = \frac{1}{\beta^2} \frac{\ln \frac{2mc^2T_o}{(h\nu_p')^2} - \beta^2 + 1 - .0235(4 - x)^{4.03}}{\ln \frac{2mc^2T_o}{(h\nu_p')^2}} . \qquad (5)$$

This expression predicts that the grain density should increase again to an asymptotic plateau value after passing through a broad minimum around $\beta_{min} = .954$. The existence of such relativistic rise to a plateau was first detected by Pickup and Voyvodic[27] and subsequently confirmed by many observations.[28-31,5,6] Shapiro and Stiller[29] made a detailed comparison of the rate of relativistic rise with theory, and obtained a very good fit to the curve which included the density effect function elaborated by Sternheimer.[25] The comparison of Eq. (5) with experiment depends critically on the knowledge of the mean ionization potential ω' for AgBr. The value for this quantity chosen here is $\omega' = 574$ eV as given by Sternheimer.[26] For the electron density in AgBr the value $n_e' = .83 \times 10^{24}$ electrons/cm^3 has been used,[20] but the knowledge of n_e' is not very critical for the present experiment, since Eq. (5) does not depend on n_e' any more except through the weak dependence on the plasma frequency. The parameter T_o is usually determined by the ratio between minimum and plateau grain densities. As will be obtained in the next section, $g^{**}_{min} = .81$ for the present experiment, which determines a value $T_o = .9$ KeV.

3. The experimental Relativistic Rise in Grain Density

The experimental ratio between the grain densities at minimum and plateau ionization, respectively, was determined in

(i) that this discrepancy is solely due to the Čerenkov contribution, which is believed to saturate very early around $\gamma = 20$ and (ii) that the estimated theoretical g* is accurate to less than a percent in this region, the above estimate follows. Of course, it should be kept in mind that the scattering measurements might have given an underestimate of $p\beta$ because of spurious scatterings. If this were indeed the case, any difference between experimental points g*-$p\beta$ and the theoretical g* would disappear, thus, reducing even further the above upper limit on the Čerenkov contribution.

4. Identity Assignments

Out of the 149 secondaries traced, 13 secondaries were identified by method a) alone, 4 secondaries by the combination of both methods a) and b), and 65 secondaries by method b) alone. Method b) was used only for those secondaries which had track lengths $\gtrsim$ 6 mm per plate and did not interact within 5 mm from the parent jet. Altogether, the analyzed portion is 55% of the traced; i.e., 82 secondaries out of 149. Figure 7 (a) shows, by a shaded histogram, the angular distribution of the secondaries which were analyzed; Figure 7 (b) shows the distribution of track length per plate for the analyzed sample; and finally, Fig. 7 (c) shows the distribution of the total track length traced for each secondary.

Method a) was used on the basis of Fig. 5. If a variation in g* along the path of a secondary was detected, a fit to each curve in Fig. 5 was attempted. The best fit to one of the curves for a given ΔR gave the identity of the secondary. The calibration of the g*-$p\beta$ function of Fig. 6 provides the

the following manner. First, the normalized grain density of a proton primary (8 TeV, $\gamma = 8.5 \times 10^3$) was observed to be $g^*_{plateau} = 1.028 \pm .024$, where the normalization is relative to the electron grain density at $\gamma \simeq 200$. The grain density at minimum ionization was determined from several of the measured pion secondaries. This corresponds to $g^*_{min} = .84 \pm .01$. The observed relativistic increase is then $(23 \pm 3)\%$. This result is compared in Table III with similar ones in previous experiments.

The theoretical function Eq. (5) of the previous section, for the choice of the critical parameters already described and for the trans-minimum region only, is reproduced in Fig. 6, where it is normalized to fit the experimental $g^*_{plateau}$. The pre-minimum part of the curve in Fig. 6 corresponds to the best fit of the g* versus R plot of Fig. 5. For this translation, use was made of the range-energy relation of Barkas.[32] As can be seen, the experimental points g*-pβ follow quite satisfactorily the slow rise to the plateau predicted by Sternheimer[26] and in this sense agree very well with the observations of Shapiro and Stiller[29] and of Barkas.[31]

The contribution from the Čerenkov radiation, which was estimated by Sternheimer[25] and Allen[33] to amount at most ~ 2% of the total increase of ionization from the minimum to the plateau, was not included in Eq. (5) of the previous section. The upper limit of this effect may be set to less than ~ 5% from the present experiment. In fact, the experimental points of jet secondaries around $\gamma = 20$ lie, on the average, at most a percent higher than the predicted g* curve of Fig. 6. Then by assuming

basis for identification by method b). As can be seen, a large number of points cluster around the pion curve, while several fit the kaon curve better. Pions were distinguished from kaons and protons in the region where the curves intercept, for the absence of a variation in g*. In any case, for each event the relative probability of it belonging to either identity was estimated and an assignment made. The identity assignment of the 82 secondaries (except 3 protons of $g^* > 1.8$) by all methods is illustrated in Fig. 6 where the black filled circles represent pions; the open circles, kaons; the open squares, protons; and a filled square, a hyperon, identified by its decay as will be reported elsewhere.[34] The secondaries, identified by method a), are reported in Fig. 6 with the same symbols as in Fig. 5. It should be pointed out that three kaons and a proton were separated by the combination of both methods a) and b) from the pions in the trans-minimum region. One of the three kaons also produced a mesic hyperfragment.

IV. EXPERIMENTAL DATA

1. Composition of Secondaries

Among the 82 secondaries analyzed, 53 were attributed to pions, 18 to kaons, 10 to protons, and one to a hyperon; this corresponds to relative frequencies of production of $(65 \pm 9)\%$, $(22 \pm 5)\%$, $(12 \pm 4)\%$, and [illegible] errors quoted are only statistical. Table VIII in Appendix II shows a breakdown of identity assignments for each event. The identity of a hyperon will be reported elsewhere.[34]

The degree of discrimination between particles in the

present set of data is shown by the two histograms in Fig. 8. The upper histogram of the two is the mass distribution of the 82 secondaries by folding the errors of g* and pβ, while the lower histogram shows the mass distribution of the identified secondaries when no errors in measurements of g* and pβ were assumed. The mass values were calculated strictly with reference to the theoretical g*-pβ curve of the pion for both cases. The similarity of shape and width in the distributions of the two histograms in Fig. 8 shows consistency in errors of measurements adopted.

It is realized that the separation is not very clear and the wrong identification is quite possible especially for those secondaries which lie in the intermediate regions between the peaks in the mass distribution in Fig. 8. An upper limit of contamination is estimated at ~ 10% of the so-called kaon and proton samples.

With the help of E_{cast} in Table I, the emission angle of each secondary was transformed into the c.m. system. The relative composition of the secondaries was found to be dependent on the c.m. emission angle $\bar{\theta}$ as shown in Table IV.

2. C.M. Momentum and Transverse Momentum Distribution

The results of the Lorentz transformation to the c.m. system are shown in Fig. 9 where the transverse momentum of the jet secondaries is plotted versus their longitudinal momentum. Figure 10 shows the momentum distributions of pion and kaon, where the shaded portion represents the secondaries with c.m. emission angles $\geq 175^{\circ}$. The average c.m. momenta of the pion and kaon are 2.1 GeV/c and 7.9 GeV/c respectively.

The ratios of the c.m. energy of the 11 baryons (10 protons, 1 Y) to half the available energy in the c.m. system corresponding to each primary, can be defined as an index of "persistency" for the baryons; Table V lists the track number, c.m. energy, half the total available energy, and index of persistency of the 11 baryons. The average of this index thus obtained (excluding 12-1) is .5 ± .2, which should not be influenced by the inaccuracy of the primary energy estimate to a good approximation. Inconsistency that the track 12-1 has an index of persistency larger than 1 might have resulted from the wrong assignment of mass for the track.

The least square fit of the pion momentum distribution, for c.m. emission angle $\bar{\theta} < 175^{\circ}$, to the form $dN \propto \bar{p}^{n}\, d\bar{p}$ gives

$$n = -.9 \pm .4, \qquad (6)$$

and the best fit is drawn in Fig. 10.

The average transverse momentum of the secondaries has been given special attention,[35] since it has been known to be small and reasonably constant through the wide range of primary energies. Figure 11 shows the transverse momentum distributions of pions, kaons, and protons where the shaded portions are for the c.m. emission angle $\bar{\theta} \geq 175^{\circ}$. The average transverse momenta of pions, kaons, and protons obtained from the present experiment are .31, .33, and [illegible]

momentum p_t = 1.3 GeV/c. Figure 12 shows the transverse momentum distribution according to the c.m. emission angle $\bar{\theta}$.

The angular dependence of the c.m. average momenta $\langle \bar{p} \rangle$

and transverse momenta $\langle p_t \rangle$ of pions, kaons, and protons are listed in Table VI. The numbers in the brackets in Table VI are the average percentage ratios of the c.m. energy to half the total available energy for secondaries in the given angular intervals where the ratios are not influenced by the inaccuracy of the primary energy estimate to a good approximation. It should be emphasized again here that the secondaries analyzed in the present experiment were selected from the outer-cone particles in the laboratory system, thus, the average values in Table VI are preferentially weighted over the large c.m. emission angles. The decrease of the transverse momentum in the extreme c.m. emission angles was noted by J. Pernegr et al.[36]

V. DISCUSSION

1. Observed Features and Theories for Jets

The present experiment has investigated the following features of high-energy jets; (i) composition of produced particles, (ii) the transverse momenta of different secondary particles, and (iii) the c.m. momentum distributions of different particles: These features are found to be dependent on the c.m. emission angle. The index of persistency, P, is related with (iv) inelasticity of interactions, η, as $P \cong 1 - \eta$. Besides these, previous extensive investigations of jets have yielded other features such as (v) variation of multiplicity of the produced shower particles versus the energy of the primary and (vi) anisotropic emission of the secondary particles in the c.m. system. So far few attempts have been made to

measure (vii) the total and elastic scattering cross sections. Investigations of some features, listed above, suffer from the inaccurate estimate of the primary energy itself.

There have been many theories proposed to explain partially or totally the observed features, listed above, such as Heisenberg's,[37] LOW's, [38] Fermi's,[39] Landau's,[40] and Bhabha's.[41] There also are phenomenological models proposed to explain certain parametric features, such as the two-center model,[42] the tunnel model,[43] and the two-fire-ball model.[44] Recently Peters' hypothesis[45] draws much attention. Amati et al.[46] developed a field-theoretical model for the multiple production of particles.

The three features (i) - (iii) of the present experiment could be studied only for two intervals of c.m. emission angle as tabulated in the Tables IV and VI; i.e., for $\bar{\theta} \geq 175^{\circ}$ and $\bar{\theta} < 175^{\circ}$. In the following section, it will be discussed that the hydrodynamical theory[40,47-54] describes the observed features consistently, as far as the K/π ratio, p_t distribution, and $\langle \bar{p} \rangle$ at $\bar{\theta} < 175^{\circ}$ are concerned. In Sect. 3 the Heisenberg theory[37,55] will be favored for interpretations of the smallness of $\langle p_t \rangle$ and high K/π ratio in the extreme c.m. emission angle $\bar{\theta} \geq 175^{\circ}$. Landau theory[40] and Heisenberg theory[37] are two extreme cases of laminar flow and turbulent flow, respectively, in the hydrodynamical system.[56] So the intermediate theory between the two extreme theories or the application of two theories to the different c.m. emission angles might be necessary to explain the overall properties of jets. (See the Sect. 4.)

2. Data for $\bar{\theta} < 175^{\circ}$ in Terms of the Fermi-Landau Theory

The basic assumption of the Fermi-Landau theory was first proposed by Fermi and later modified by Landau. When the two very fast nucleons collide, the energy in the c.m. system is released in a very small volume Ω

$$\Omega = \frac{4}{3}\left(\frac{\hbar}{m_{\pi}c}\right)^3 \frac{2m_i c^2}{\bar{E}_o} \tag{7}$$

where m_i is the nucleon's mass and $\bar{E}_o$ is the total energy of the two colliding nucleons in the c.m. system, and the Lorentz' contraction in the direction of the nucleon's motion is taken into account. The nuclear interaction is "strong", the interaction volume Ω is small and the energy distribution will be determined by statistical laws. Fermi originally took this initial stage of statistical equilibrium as "frozen" and the observed final state of multiple production process reflected just such equilibrium. Landau modified the view to that the observed number of particles in a nuclear interaction does not correspond to the first stage of statistical equilibrium but to the second stage when a critical temperature has been reached. Namely, when due to the expansion of the system the mean free path of the created particles becomes comparable with the linear dimension of the system and their mutual interactions decrease sharply. In the process of expansion the system can be visualized as a relativistic hydrodynamical system, since the mean free path remains small compared with the dimension of the system.

According to the theory, the particle density of the Boson gas ρ at the critical temperature, T_c, at a certain

section of the system is expressed by

$$\rho = \Sigma_i \rho_i$$
$$\rho_i = (g_i/2\pi^2)(kT_c/c\hbar)^3 F(m_i c^2/kT_c) \tag{8}$$

where

$$F(x_c) = x_c^2 \sum_{\nu=0}^{\infty} \frac{K_2[(1+\nu)x_c]}{(1+\nu)}$$

$$x_c = m_i c^2/kT_c,$$

g_i is the statistical weight of the particle of mass m_i and $K_2(x)$ is a modified Bessel function of the second order.[48,57] The $K^{\pm}/\pi^{\pm}$ ratio as predicted by Eq. (8) as a function of $x_c = m_\pi c^2/kT_c$, is shown in Fig. 13 where $g_{K^{\pm}} = g_{\pi^{\pm}} = 2$ is assumed. From the present experimental ratio of the number of charged kaons to that of charged pions, .34 ± .09,

$$kT_c = (1.3 \pm .2)m_\pi c^2. \tag{9}$$

If the $K^{\pm}/\pi^{\pm}$ ratio for $\bar{\theta} < 175^\circ$ is considered (9/46 = .20 ± .07), then

$$kT_c = (.93 \pm {}^{.18}_{.15})m_\pi c^2. \tag{10}$$

The hydrodynamical theory further predicts the energy density of the produced Boson particles at a temperature T as

$$\epsilon_i(T) = (g_i kT/2\pi^2)(kT/c\hbar)^3 G(m_i c^2/kT) \tag{11}$$

where

$$G(x) = x^2 \sum_{\nu=0}^{\infty} \frac{1}{1+\nu}\left[\frac{3K_2(<1+\nu>x)}{1+\nu} + xK_1(<1+\nu>x)\right],$$

$$x = m_i c^2/kT,$$

and $K_1(x)$ is a modified Bessel function of the first order.[48,57] So the energy per particle at the critical temperature, T_c, becomes

$$\bar{E}_i = \epsilon_i(T_c)/\rho_i(T_c)$$

$$= kT_c\ G(m_i c^2/kT_c)/F(m_i c^2/kT_c). \qquad (12)$$

A graph of this function at various $x_c = m_\pi c^2/kT_c$ is shown in Fig. 14 for kaons and pions, as calculated from Refs. 48 and 57. Also shown is the ratio of $\bar{E}_K$ to $\bar{E}_\pi$, which stays around unity for $kT_c >> m_\pi c^2$, and goes up, in a complicated manner, eventually to $3.54 = m_K/m_\pi$ in the non-relativistic limit. The overall average momenta of kaons and pions ($\langle\bar{p}_K\rangle$ = 7.9 GeV/c, $\langle\bar{p}_\pi\rangle$ = 2.1 GeV/c) are rather large when Eq. (12) gives $\bar{E}_K$ = .77 GeV and $\bar{E}_\pi$ = .46 GeV at $kT_c = m_\pi c^2$. This would immediately suggest an explanation in terms of higher critical temperature than $m_\pi c^2$ as seen from Fig. 14. The same situation persists even if the average momenta of kaons and pions for $\bar{\theta} < 175^\circ$ are only taken into consideration. While it may not be ignored that the over-estimates of the primary energies, in general, result in those of the c.m. momenta proportionally through the Lorentz factor $\gamma_{cast} = \sqrt{E_{cast}/2m_p c^2}$, another natural explanation could be given by assuming that a portion of the fluid, that is responsible for the isotropic emission of pions and kaons according to Eq. (12), has a c.m. velocity $\bar{\beta}$. While $kT_c = m_\pi c^2$, the average c.m. momenta of kaons and pions will reach the same magnitude as the present data for $\bar{\theta} < 175^\circ$ if $\bar{\beta}$ = .88 ($\bar{\gamma}$ = 2.1). Moreover, the ratio of the c.m. average momenta of kaons and pions 1.5 ± .5 is consistent with

$$kT_c = m_\pi c^2, \qquad (13)$$

since it can be shown that the ratio of average momenta of kaons and pions is approximately Lorentz invariant provided that $\bar{\beta} > .3$

and that kaons and pions are emitted isotropically in the fluid.

The transverse momentum distributions are consistent with a critical temperature $kT_c \simeq m_\pi c^2$. The overall distribution of pion transverse momentum shows very good agreement with the calculations (for $kT_c = m_\pi c^2$) of Milečin and Rozental[50] and Milekhin[51] as the experiments of Debenedetti et al.[58] and Hansen et al.[59] previously showed. The transverse momentum distribution of pions for $\bar{\theta} < 175^\circ$ is shown in Fig. 15, together with the theoretical calculations by Milekhin[51] for the two parameters $kT_c = m_\pi c^2$ and $\sinh \xi = 0$ and .5, where ξ is defined as the hydrodynamical transverse velocity at the moment of break-up. The best fit obtains when

$$kT_c = m_\pi c^2 \text{ and } \sinh \xi = 0, \tag{14}$$

which means the transverse velocity at the moment of break-up is negligible. Thus, the one-dimensional hydrodynamical theory gives an overall satisfactory fit to the data for this angular interval. Here it must be reminded that Eq. (6) is also consistent with $n = -1$, which is predicted by the hydrodynamical theory.

3. Data for $\bar{\theta} \geq 175^\circ$ and Their Interpretations

Several disagreements emerge when K/π ratio, the average momenta of pions and kaons, and the transverse momenta for $\bar{\theta} \geq 175^\circ$ are studied under the light of the hydrodynamical theory. The large $K^\pm/\pi^\pm$ ratio (9 K versus 7 π) suggests a large critical temperature of the fluid (Fig. 13)

$$kT_c \gg m_\pi c^2 \tag{15}$$

while the small transverse momenta observed in this angular region can only be explained in terms of the critical temperature $kT_c << m_\pi c^2$. The average c.m. momenta are affected too much by several high-energy mesons, and the ratio of the c.m. momenta of kaons and pions will not help to clarify the situation.

The smallness of the transverse momenta in the region of extreme backward emission is suggestive of the Heisenberg theory since this theory predicts

$$p_t \approx m_\pi c. \tag{16}$$

Moreover, the high concentration of kaons in the extreme emission angle is also consistent with this theory.[60] The overall ratio of kaon production to pion (.34 ± .09) is consistent with what the Heisenberg theory predicts; i.e., .29, taken from Table 3. 1 of Ref. 55 for $E_o/M = 10^3$. The large c.m. momenta may be attributed to the high velocity of the disturbance wave. But this theory can not explain the large transverse momenta for $\bar{\theta} < 175^\circ$. The internal consistency of the interpretation in the previous section might favor definitely the hydrodynamical theory for the data for $\bar{\theta} < 175^\circ$.

4. Correlation Between the Different Interpretations

Milekhin[61] clarified the inter-relation between the Landau and Heisenberg theory in the hydrodynamical theory. Originally Landau assumed, as an additional postulate to his theory, the equation of state

$$p = c_o^2 \epsilon, \tag{17}$$

where p is the pressure, ϵ the energy density, c_o^2 the square of the sound velocity of the medium in unit of the velocity of light

$$c_o^2 = 1/3 \qquad (18)$$

from an analogy with the black body radiation. But it turned out that when

$$c_o^2 = 0 \qquad (19)$$

the hydrodynamical description becomes equivalent to the Heisenberg theory. Since the data for $\bar{\theta} \geq 175^\circ$ in the present experiment favor an interpretation in terms of Heisenberg theory and those for $\bar{\theta} < 175^\circ$ in terms of Landau theory, then it might be concluded that c_o^2 either varies according to the c.m. emission angle or is some number between 0 and 1/3. But it seems clear that the two views are sufficient to describe the parametric features observed in the present experiment.

VI. CONCLUSIONS

The present experiment has made full use of the large dimension of the stack, which revealed extremely valuable both in the tracing of tracks and in the observation of the gradual change of ionization as the secondaries traversed the block of emulsion. Moreover, the local normalization of the grain density to that of high-energy electrons and the large statistics of grain counts contributed to improve the method of identity assignment. The present experiment shows good agreement with the theory of ionization loss in the trans-minimum region, to an extent which enabled discrimination of kaons from pions up to $p\beta$ of ~ 10 GeV/c.

Among 82 secondaries analyzed, the composition found consisted of 53 pions, 18 kaons, 10 protons, and one hyperon. The average c.m. momenta were 2.1 and 7.9 GeV/c for pions and

kaons respectively in the solid angle analyzed; the transverse momenta were .31, .33, and .35 GeV/c, respectively, for pions, kaons, and protons. The overall results of the present experiment may be roughly accounted for by the hydrodynamical theory with a critical temperature $kT_c = m_\pi c^2$, consistent with the observed average K/π ratio and the transverse momenta.

The baryons carried, on the average, a fraction .5 ± .2 of the available energy per nucleon in the c.m. system of the collision. This method, if refined further with better statistics, is a good means of measurement of inelasticity of nuclear interaction of high-energy jets since it is not affected by the accuracy of the primary energy estimate to a good approximation. From analysis of the four-momentum transfer of the 11 baryons by assuming that the identified baryons are surviving target nucleons, it has been inferred that the peripheral or multipheral models[46] of high-energy interactions disagree with the observation of $\sqrt{-\Delta^2} = 1.1$ GeV.[62] This conclusion may coincide with the central character of inelastic nuclear processes, deduced from the present experiment.

Even if the number of tracks analyzed is small, the qualitative structure observed in the extreme backward region of c.m. emission angle is conspicuous. The observed features are as follows: (i) for $\bar{\theta} \geq 175^\circ$, there were 7 π, 9 K, 10 p, and 1 Y; for $\bar{\theta} < 175^\circ$, there were 46 π, 9 K, and no baryons; (ii) for $\bar{\theta} \geq 175^\circ$, the average c.m. momenta of pions and kaons were 8.5 and 14.3 GeV/c respectively; for $\bar{\theta} < 175^\circ$, they were 1.1 and 1.5 GeV/c respectively; (iii) for $\bar{\theta} \geq 175^\circ$, the transverse momenta were .20, .21, and .35 GeV/c, respectively, for

pions, kaons, and protons; for $\bar{\theta} < 175^{\circ}$, those of pions and kaons were .32 and .46 GeV/c respectively. And the increase of transverse momentum with the mass of the secondary particle is noticeable.

For the observed features in $\bar{\theta} < 175^{\circ}$, the hydrodynamical theory with $kT_c = m_\pi c^2$ describes consistently except the fact that the average c.m. velocity of the fluid that is responsible for the isotropic emission of mesons must be assumed around $\bar{\beta} = .88$ ($\bar{\gamma} = 2.1$), to get the magnitude of the average c.m. momenta observed. The fact that the c.m. momentum distribution of pions is the form $dN \propto \bar{p}^n \, d\bar{p}$ with $n = -.9 \pm .4$ supports this view. But for $\bar{\theta} \geq 175^{\circ}$ the transverse momenta become smaller, the c.m. momenta larger, and the K/π ratio is around unity. So for the latter region, interpretations in terms of the Heisenberg theory are favored.

The existence of several very high-energy secondary mesons in the extreme c.m. angle must be examined with better statistics. These mesons may be the decay products of the "persistent" excited nucleon states. Or phenomenologically, they may have the function of the energy carrier, which is built in the hydrodynamical theory to carry away about a half of the available energy in c.m. system.[49]

The theoretical correlation between the two extreme views were discussed by Milekhin.[61] The consequences of the present view that both the Landau and Heisenberg theories might contribute may yield a variation of the multiplicity of shower particles n_s as a function of the primary energy E_o of the form:

$$n_s = a \, E_o^{1/4} + b \, E_o^{1/2}$$

where a and b are constants. The total cross section of interaction would increase slightly by consequence of the Heisenberg part. The ratio of kaon production to that of pion would not vary very much from the known rate of production at accelerator energies.

VII. ACKNOWLEDGEMENTS

The author wishes to express his hearty gratitude to his thesis adviser Prof. R. Levi Setti whose guidance has been invaluable throughout the course of the present work. He is also much indebted to Prof. M. Koshiba of the University of Tokyo who originally recommended the present project and gave generous help during the initial phase of the work. He is grateful to Dr. C. H. Tsao for helpful discussions and check of numerical calculations through the computer. Thanks are due to Drs. J. Kidd, F. Abraham, and K. Rybicki for helpful criticism and valuable discussions. Discussions with Prof. Y. Nambu, Dr. K. Mori, and Prof. J. Gierula were deeply appreciated by the author. Mrs. J. Para was very helpful in the tracing. Mr. D. Spector was appreciated for calculations of the mass spectrum through IBM 7094. He is very grateful to Miss B. Gygi, Mr. L. Henry, Mr. P. Li, Mrs. I. Orr, Mr. G. Schultz, and Mr. P. Waltz for their assistance in tracing and analysis. Our thanks are also due to Dr. J. Hornbostel [illegible] National Laboratory for the loan of a Koristka digitized scattering microscope.

LIST OF REFERENCES

[1] M. Koshiba, "Interactions of 10^{12} ev Energy Range," BNL 772 (T-290), Brookhaven National Laboratory, Upton, New York, p 18 (1961); "Recent Large Stack Investigations of High Energy Jets," Proceedings of International Conference on Cosmic Rays at Jaipur, India, (1963).

[2] D. H. Perkins, Progress in Elementary Particle and Cosmic Ray Physics, Vol. V, North-Holland Publishing Co., Amsterdam, p 257 (1960); International Conference on Theoretical Aspects of Very High-Energy Phenomena, 1961, CERN Scientific Information Service, Geneva, p 97 (1961).

[3] V. T. Cocconi, T. Tazzini, G. Fidecaro, M. Legros, N. H. Lipman, and A. W. Merrison, Phys. Rev. Lett. 5, 19 (1960); G. Cocconi, Proceedings of the 1960 Annual International Conference on High Energy Physics at Rochester, Interscience Publishers, Inc., New York, p 800 (1960); L. Gilly, B. Leontic, A. Lundby, R. Mennier, J. P. Stroot, and M. Szeptycka, ibid, p 837; W. F. Baker, R. L. Cool, E. W. Jenkins, T. F. Kycia, S. J. Lindenbaum, W. A. Love, D. Lüers, J. A. Niederer, S. Ozaki, A. L. Read, J. J. Russell, and L. C. L. Yuan, Phys. Rev. Lett. 7, 101 (1961); V. L. Fitch, S. L. Meyer, and P. A. Piroué, Phys. Rev. 126, 1849 (1962); A. Schwarzschild and Č. Zupančič, Phys. Rev. 129, 854 (1963).

[4] H. Filthuth, Aix-en-Provence International Conference on Elementary Particles, p 93, (1961).

[5] R. R. Daniel, J. H. Davies, J. H. Mulvey, and D. H. Perkins, Phil. Mag. 43, 753 (1952).

[6] B. Edwards, J. Losty, K. Pinkau, D. H. Perkins, and J. Reynolds, Phil. Mag. 3, 237 (1958).

[7] F. Brisbout, C. Dahanayake, A. Engler, P. Fowler, and P. Jones, Nuovo cimento, 3, 1400 (1956).

[8] A. G. Barkow, B. Chamany, D. M. Haskin, P. L. Jain, E. Lohrmann, M. W. Teucher, and M. Schein, Phys. Rev. 122, 617 (1961).

[9] P. L. Jain, Phys. Rev. 122, 1890 (1961); Nuovo cimento 24, 698 (1962).

[10] J. Kidd, Nuovo cimento 27, 57 (1963).

[11] M. Teucher, E. Lohrmann, D. H. Haskin, and M. Schein, Phys. Rev. Lett. 2, 313 (1959).

[12] P. L. Jain, Phys. Rev. 125, 679 (1962).

[13] J. Gierula, D. M. Haskin, and E. Lohrmann, Phys. Rev. 122, 626 (1961).

[14] E. Lohrmann, M. W. Teucher, and M. Schein, Phys. Rev. 122, 672 (1961).

[15] E. Lohrmann, Phys. Rev. 122, 1908 (1961).

[16] A. Bonetti, C. Dilworth, G. P. S. Occhialini, Bull. Univ. Bruxelles, No. 13 b (1951).

[17] By the courtesy of Prof. W. H. Barkas.

[18] C. Castagnoli, G. Cortini, D. Moreno, C. Frazinetti, and A. Manfredini, Nuovo cimento 10, 1539 (1953).

[19] B. Rossi, High-Energy Particles, Prentice-Hall, New York, p 24 (1952).

[20] M. M. Shapiro, Handbuch der Physik, Vol. XLV, Springerverlag, Berlin, p 342 (1958).

[21] C. F. Powell, P. H. Fowler, and D. H. Perkins, The Study of Elementary Particles by the Photographic Method, Pergamon Press, London (1959).

[22] H. Messel and D. M. Ritson, Phil. Mag. 41, 1129 (1950).

[23] M. Schönberg, Nuovo cimento 8, 159 (1951).

[24] L. Brown, Phys. Rev. 90, 95 (1953).

[25] R. M. Sternheimer, Phys. Rev. 88, 851 (1952); Phys. Rev. (L), 89, 1148 (1953); Phys. Rev. 91, 256 (1953); Phys. Rev. (E), 93, 1434 (1954); Phys. Rev. 93, 351 (1954).

[26] R. M. Sternheimer, Phys. Rev. 103, 511 (1956). This paper takes into consideration of the determination of the mean excitation potential I by Caldwell (D. O. Caldwell, Phys. Rev. 100, 291 (1955)) as $I = 13\ Z$ in contrast to $I = 9.4\ Z$ in Ref. 25.

[27] E. Pickup and L. Voyvodic, Phys. Rev. (L), 80, 89 (1950).

[28] H. A. Morrish, Phil. Mag. 43, 533 (1952).

[29] M. Shapiro and B. Stiller, Phys. Rev. (L), 87, 682 (1952); Phys. Rev. 92, 735 (1953).

[30] G. Alexander and R. H. W. Johnston, Nuovo cimento 5, 363 (1957)

[31] J. W. Patrick and W. H. Barkas, Suppl. Nuovo cimento 23, 1 (1962).

[32] W. H. Barkas, UCRL 3384 (1956); B. H. Willis and C. V. Stableford, UCRL 2426 (rev.) (1956).

[33] J. R. Allen, Phys. Rev. (L) 93, 353 (1954).

[34] A possible evidence of the new hyperon $Y^{(-)}$ ($\not\rightarrow K^{(-)} + \Lambda_o$) will be published in a separate paper.

[35] J. Nishimura, Soryushiron Kenkyu 12, 24 (1956); Z. Koba, Proceedings of 1956 Annual International Conference on High-Energy Physics at Rochester, Interscience Publishers, Inc., New York, p IV-46 (1956); A. Debenedetti, C. M. Garelli, L. Tallone and M. Vigone, Nuovo cimento 4, 1143 (1956); B. Edwards et al., Ref. 5; O. Minakawa, Y. Nishimura, M. Tsuzuki, H. Yamanouchi, H. Aizu, H. Hasegawa, Y. Ishii, S. Tokunaga, Y. Fujimoto, S. Hasegawa, J. Nishimura, K. Niu, K. Nishikawa, K. Imaeda, and M. Kazuno, Suppl. Nuovo cimento 11, 125 (1959); M. Schein, D. M. Haskin, E. Lohrmann, and M. Teucher, Phys. Rev. 116, 1238 (1959); L. F. Hansen and W. B. Fretter, Phys. Rev. 118, 812 (1960).

[36] J. Pernegr, V. Šimák, and M. Votruba, Nuovo cimento 17, 129 (1960).

[37] W. Heisenberg, Z. Phys. 113, 61 (1939); 126, 569 (1949); 133, 65 (1952).

[38] H. W. Lewis, J. R. Oppenheimer, and S. A. Wouthuysen, Phys. Rev. 73, 127 (1949).

[39] E. Fermi, Progr. Theor. Phys. 5, 570 (1950); Phys. Rev. 81, 683 (1951); 92, 452 (1953); 93, 1434 (1954).

[40] L. D. Landau, Izv. Akad. Nauk SSSR 17, 51 (1953).

[41] H. J. Bhabha, Proc. Roy. Soc. A 152, 559 (1953).

[42] E. L. Feinberg and D. S. Černavsky, Dokl. Akad. Nauk SSSR 81, 795 (1951); S. Takagi, Progr. Theor. Phys. 7, 123 (1952); W. L. Kraushaar and L. J. Marks, Phys. Rev. 93, 326 (1954).

[43] F. C. Roesler and C. B. A. McCusker, Nuovo cimento 10, 127 (1952); G. Cocconi, Phys. Rev. 93, 1107 (1954).

[44] K. Niu, Utyusen-Kenkyu, 3, 85 (1958); Nuovo cimento 10, 994 (1958); P. Ciok, T. Coghen, J. Gierula, R. Holynski, A. Jurak, M. Miesowicz, T. Saniewska, O. Stanisz, and J. Pernegr, Nuovo cimento 8, 166 (1958); G. Cocconi, Phys. Rev. 111, 1699 (1958).

[45] B. Peters, Nuovo cimento 23, 88 (1963); 1962 International Conference on High-Energy Physics at CERN, CERN Scientific Information Service, Geneva, p 623 (1962).

[46] D. Amati, S. Fubini, A. Stanghellini, and M. Tonin, Nuovo cimento 22, 569 (1961); 26, 896 (1962).

[47] S. S. Belen'kij and L. D. Landau, Suppl. Nuovo cimento 3, 15 (1956).

[48] Z. Koba, Progr. Theor. Phys. 15, 461 (1956).

[49] S. Amai, H. Fukuda, C. Iso, and M. Sato, Progr. Theor. Phys. 17, 241 (1957).

[50] G. A. Milečin and I. L. Rozental, Suppl. Nuovo cimento 8, 770 (1958).

[51] G. A. Milekhin, Soviet Physics JETP 35 (8), 682 and 829 (1959).

[52] E. L. Feinberg, Ninth International Annual Conference on High-Energy Physics at Kiev, Vol. II, p 358 (1959); Usp. Fiz. Nauk 70, 333 (1960); Soviet Physics (Uspekhi) 3, 159 (1960).

[53] C. Iso, K. Mori, and M. Namiki, Progr. Theor. Phys. 22, 403 (1959).

[54] D. S. Chernavsky and E. L. Feinberg, "Cosmic Rays and the Theory of Strong Interactions," International Conference on Cosmic Rays at Jaipur, India (1963).

[55] Z. Koba, Progr. Theor. Phys. 17, 288 (1957).

[56] D. Czernawski, Postepy Fizyki 9, 653 (1958).

[57] S. Z. Belen'kij, Dokl. Akad. Nauk SSSR 99, 523 (1954).

[58] A. Debenedetti et al. in Ref. 35.

[59] L. F. Hansen et al. in Ref. 35.

[60] S. Hayakawa, Soryushiron Kenkyu 12, 1 (1956). Table 1 by Z. K.

[61] G. A. Milekhin, Proceedings of 1959 International Conference on High-Energy Physics, Vol. II, p 397 (1959).

[62] R. W. Huggett, K. Mori, C. O. Kim, and R. Levi Setti, "Some Properties of Very High-Energy Inelastic Processes Deduced from Measurements on the Surviving Target Nucleon," International Conference on Cosmic Rays at Jaipur, India (1963).

APPENDIX I

1. Grain Density Measurements

Grain counting was performed with 53X objective and 12.5X ocular. As discussed in Chapt. III, the convention for counting is very critically relevant to the ratio of the plateau to the minimum, which, in turn, sets the δ-ray energy limit T_o. In the convention adopted here, those grains which were not strictly aligned with the particle path, were rejected in counting, but even small grains were counted if they aligned well. Repeated observations of the grain counts over the same track by the same observer showed consistently the same value within 0.2% over a substantial elapse of time. The grain density was not measured within 1 cm from the plate edges. Unfortunately, the grain density varied from one plate to another and had a dependence on the depth of emulsion as already shown in Figs. 1 and 2. The grain density of a secondary, g, was normalized to the average grain density of high-energy electrons, g_o. This procedure was carried out effectively by counting the grains through a whole plate from the glass bottom to the air surface of the emulsion, both for the secondary and for the high-energy electron tracks. This normalized grain density, $g^* = g/g_o$, was obtained by individual observers to eliminate subjective factors in the counting procedure. The grain density of flat secondaries was normalized to that of the high-energy electrons at the same depth of the emulsion in the vicinity of the secondary, after constructing a curve similar to that shown in Fig. 2. The elctron tracks were carefully

selected and low-energy tracks were discarded. The radiative correction[63] was inferred as negligible from the measurements of the normalized grain density of the highest-energy electrons in the cores of jets ($\gamma \geq 4 \times 10^3$), $g^* = .99 \pm .03$, where the normalizing procedure was the same as for the secondaries by using the shower electrons ($\gamma \simeq 200$). The average grain density of shower electrons, g_o, from different showers in a given plate showed consistently the same value. The values of g^* for the same track for several successive plates usually showed good regularity. Errors on g^*, Δg^*, were taken as

$$\Delta g^* = \sqrt{1/N_g + 1/N_{g_o}}$$

where N_g and N_{g_o} are the number of grains counted, respectively, for the secondary and high-energy electron tracks.

2. Scattering Measurements

The multiple scattering measurements were made on Koristka R-4 and MS-2 microscopes with 100X and 90X objectives with a total magnifying power of about 1200X; the microscope lamp was always turned on two hours before measurement. Scattering measurements were not performed if the secondary was within about 4 cm from the plate edges. The standard Sagitta method[20,21] was used to obtain $p\beta$. For the present experiment the value of the scattering constant K was taken to be 26.7, 27.6, 28.5, and 29.3, respectively, for 250 microns, 500 microns, 1000 microns, and 2000 microns cells.[64] This value K refers to $\beta = 1$ with the cutoff procedure, which means that the second differences that exceed the values of four times the average are eliminated in the next average-taking procedure. In

practice, the measured second differences, $\langle D_2(1)\rangle_{meas.}$, contain contributions from effects other than multiple Coulomb scattering. Among these effects[65] the combined effects of stage noise and reading noise were estimated from measurements of second differences on a Bausch and Lomb straight line. The combination of spurious scattering with the stage noise, reading noise, and grain noise were estimated from scattering measurements on flat primary tracks of high energy. Results of these measurements are tabulated in Table VII. As seen in this table, while the stage noise is almost independent of the cell size, other listed noises are probably due to small gradual distortions of the plates in packing and due to the differential shrinkage of emulsion during processing. Some effect might come from the fact the average second differences listed for larger cell lengths resulted from taking completely overlapping second differences from the measurements for the basic cell length rather than taking the direct measurements for the actual cell lengths.

The noise elimination was carried out on the assumption that the noise contribution, ϵ, is independent of cell length, as follows:

$$\langle D_2(1)\rangle^2_{meas.} = \epsilon^2 + \left(\frac{K(1)t_1^{3/2}}{573\ p\beta}\right)^2 \qquad (20)$$

where $\langle D_2(1)\rangle_{meas.}$ is the average second difference of the basic cell length t_1,

$$\langle D_2(n)\rangle^2_{meas.} = \epsilon^2 + \frac{K^2(n)n^3}{K^2(1)}\left(\frac{K(1)t_1^{3/2}}{573\ p\beta}\right)^2 \qquad (21)$$

where $\langle D_2(n)\rangle_{meas.}$ is the average second difference by the

completely overlapping procedure of the cell length nt_1. Then from Eqs. (20) and (21)

$$\langle D_2(1)\rangle = \frac{K(1)t_1^{3/2}}{573\ p\beta}$$

$$= \frac{\sqrt{\langle D_2(n)\rangle^2_{meas.} - \langle D_2(1)\rangle^2_{meas.}}}{\sqrt{(K(n)/K(1))^2 n^3 - 1}}. \qquad (22)$$

The basic cell length used was 250 microns or 500 microns in this experiment. The errors of the final values were processed according to Di Corato et al.,[66] whose methods were based on the theory of D'Espagnat.[67] In most of the cases the actual error was either $1.46/\sqrt{n_D}$ for n = 2 or $1.92/\sqrt{n_D}$ for n = 4, where n_D is the number of second differences of the basic cell length. For each secondary, the two sets of values of pβ and its error were processed by a combination of $\langle D_2(2)\rangle_{meas.}$ and $\langle D_2(1)\rangle_{meas.}$ or by that of $\langle D_2(4)\rangle_{meas.}$ and $\langle D_2(1)\rangle_{meas.}$ through Eq. (22), and they were examined for consistency of measurements. In a few cases, when the two values of pβ of the same secondary, which were obtained as described above, were not in agreement within their errors, then the value of pβ and its error, which were obtained through the conbination of n = 4 and n = 1 values, were adopted. The third differences were processed in the similar way to get pβ.[66] The average ratio of pβ deduced from the third differences and that from the secondary differences on the same track were .99, which shows, on the average, there are not serious distortions in the stack. All these values of pβ were also tested of their consistency with those that were obtained independently by eliminating the total noise assuming the noise of the

corresponding cell length listed in Table VII.

REFERENCES FOR APPENDIX I

63 K. I. Alekseyeva, G. B. Zhdanov, E. A. Zamchalova, M. Novak, M. I. Tretyakova, and M. N. Shcherbakova, Proceedings of the 3rd International Conference on Nuclear Photography, Moscow, 1962, p 396; G. B. Zhdanov, M. I, Tret'yakova, V. N. Tsytovich, and M. N. Shcherbakova, Soviet Physics JETP 43 (16), 245 (1963).

64 C. Fichtel and M. W. Friedlander, Nuovo cimento 10, 1032 (1958).

65 R. Levi Setti, Nuovo cimento 8, 96 (1951).

66 M. Di Corato, B. Locatelli, and D. Hirschberg, Suppl. Nuovo cimento 4, 448 (1956).

67 B. D'Espagnat, Compt. Rend. Acad. Sci. 232, 800 (1951).

APPENDIX II

Table VIII

TABLE I

Events Studied

Event No.	Type	E_{cast} (TeV)	E_{ch}	σ	Dip mm/p	Potential Jet Axis (cm)
4	$2 + 17_p$	5.7	1.5	.93	10.5	26
5	$2 + 5_p$	-	2.4	-	3.4	25
8	$0 + 41_\alpha$	3.3	4.2	.84	218	25
9	$1 + 11_p$	.60	.22	.76	2.9	45
12	$2 + 23_p$	9.9	3.7	1.03	3.2	32
13	$3 + 33_p$	2.5	2.2	.76	4.6	40
23	$3 + 18_n$	5.4	.93	.71	2.4	44
28	$1 + 23_p$	3.0	3.4	.98	11	31
41	$3 + 15_\alpha$	.24	.14	.71	3.7	23
46	$3 + 41_\alpha$	.33	.78	.67	2.8	31
47	$2 + 14_p$	12	1.8	.92	293	41
49	$0 + 9_p$	1.7	.43	.81	14.8	30
59	$3 + 68_\alpha$	11	6.9	.69	7.6	60
63	$2 + 20_p$	6.6	1.7	.65	6.1	37
72	$1 + 27_p$	15	1.8	.65	2.6	21
77	$3 + 43_\alpha$	.67	1.3	.74	47.3	22
109	$1 + 20_\alpha$	2.8	.66	.57	2.0	35
113	$0 + 4_\alpha$	-	8.2	-	7.2	24
116	$0 + 8_p$	.23	.58	.49	78.2	44
117	$0 + 17_p$	1.5	.70	.67	4.3	32
118	$0 + 21_p$	15	2.2	.69	476	28
120	$2 + 23_p$	6.2	3.2	1.11	2.1	34
Average		5.2	2.2	.77		

TABLE II

Tracks Traced

Event No.	Numbers Traced	Inter-acted	Out of Stack	Lost	Length Followed (cm)	
4	9	2	2	5	136.3	1' mesic hyperfragment among tertiary products
5	1	1	-	-	6.3	
8	17	10	5	1	269.5	A pion scatters 4.5°
9	3	1	2	-	50.6	
12	7	6	1	-	75.4	
13	7	3	2	2	174.9	
23	3	2	1	-	51.0	
28	6	2	1	2	33.3	A track scatters 13.3° at .184 cm
41	4	1	1	2	29.6	
46	5	2	1	2	104.4	
47	6	3	1	2	63.7	
49	7	4	3	-	136.6	
59	16	10	6	-	267.9	
63	4	1	2	1	10.1	
72	5	3	1	-	44.4	A proton stops
77	17	5	10	2	164.9	A track scatters 11.2° at .9 cm
109	4	3	1	-	110.5	
113	4	3	1	-	40.2	
116	5	3	1	1	63.9	
117	5	3	2	-	76.1	
118	9	5	2	2	109.4	
120	5	1	-	4	21.1	A hyperon decays in flight
	149	74	46	26	2040.1	

TABLE III

The Ratio of the Asymptotic Plateau Value to the Minimum Grain Density

Author	Ratio	Type of Emulsion	Highest γ for Calibration
Pickup et al.[a]	1.10	G-5	~20
Morrish[b]	1.05	G-5	~25
Daniel et al.[c]	1.10	G-5	~20
Shapiro et al.[d]	1.14 ± .03 (1.16 ± .03)	G-5	3400 (>300)
Alexander et al.[e]	1.133 ± .008	G-5	~500
Edwards et al.[f]	1.08	(G-5?)	?
Patrick et al.[g]	1.18	K-5, G-5	1400
Present work	1.23 ± .03	G-5	10^4

[a]Ref. 27; [b]Ref. 28; [c]Ref. 5; [d]Ref. 29; [e]Ref. 30; [f]Ref. 6; [g]Ref. 31.

TABLE IV

Relative Composition of the Secondaries versus $\bar{\theta}$

Range of C.M. Angle	Numbers			
	Pion	[illegible]	Proton	[illegible]
$\bar{\theta} \geq 175^\circ$	7	9	10	1
$\bar{\theta} < 175^\circ$	46	9	-	-
Overall	53	18	10	1

TABLE V

Index of Persistency

Track No.	Identity	C.M. Energy	$m_p\gamma_{cast}$	Index of Persistency
4-15	p	15.1 GeV	52 GeV	.29
8-1	p	29.3	39	.75
8-28	p	8.6	39	.22
9-1	p	5.1	17	.30
12-1	p	73.9	68	1.09
13-1	p	8.5	35	.24
41-2	p	7.8	10	.78
59-2	p	17.3	72	.24
72-G1	p	66.7	83	.80
109-7	p	10.8	37	.29
120-1	Y	38.4	53	.72
Average		25.6	(Excluding 12-1)	.46 ± .15

TABLE VI

Angular Dependence of the Average C.M.

Momentum and Transverse Momentum

Range of C.M. Angle $\bar{\theta}$	$\langle\bar{p}\rangle$ (GeV/c)			$\langle p_t\rangle$ (GeV/c)		
	π	K	p	π	K	p
$\bar{\theta} \geq 175^\circ$	8.5 (11%)*	14.3 (23%)	26 (52%)	.20 ± .08**	.21 ± .07	.35 ± .11
$\bar{\theta} < 175^\circ$	1.1 (3.6%)	1.5 (9.7%)		.32 ± .05	.46 ± .15	-
Overall	2.1	7.9	26	.31	.33	.35

*Average precentage ratio of the c.m. energy to half the total available energy in the c.m. system.

**Errors are only statistical.

TABLE VII

The Noise Level by Second Differences in Microns

Cell Length t	By Primaries	By Straight Line in MS-2
250 microns	.107 ± .003*	
500	.112 ± .008 (.124)**	(.059 ± .008)
1000	.165 ± .017 (.160)	(.078 ± .014)
2000	.298 ± .079 (.240)	(.086 ± .022)

*Errors quoted are only statistical.

**The numbers in the brackets are for MS-2.

TABLE VIII

Breakdown of Identity Assignments

Track No.[a]	tan θ_i	g_1^*	ΔR(cm)	g_2^*	pβ	Identity	Method used	p_t
4-3	.043	.95±.02	-	-	9.6 ±3.9	K	b)	.413
4-12	.008	.96±.04	-	-	$6.5^{+3.7}_{-2.9}$	π	b)	.052
4-14	.105	.92±.03	23	1.07±.06	$.71^{+.38}_{-.28}$	K	a),b)	.086
4-15	.11	.94±.03	-	-	$1.3^{+1.0}_{-.7}$	p	b)	.167
4-16	.175	.93±.03	23	1.01±.04	$1.0^{+.4}_{-.3}$	K^-	a),b)	.194
4-17	.232	.97±.03	-	-	$2.4^{+1.3}_{-1.0}$	π	b)	.543
8-1	1.08	1.88±.06	2.6	2.28±.07	.37± .02	p	a)	.477
8-4	.153	.91±.03	-	-	1.21± .25	π	b)	.184
8-5	.161	.90±.04	-	-	2.53± .51	π	b)	.403
8-6	.070	.97±.02	-	-	2.51± .50	π	b)	.176

TABLE VIII

(continued)

Track[a] No.	tan θ_i	g_1^*	ΔR(cm)	g_2^*	$p\beta$	Iden-tity	Method used	p_t
8-7	.067	.93±.04	-	-	2.9 ± .7	π	b)	.194
8-8	.082	.96±.04	-	-	4.5 ±1.6	π	b)	.368
8-9	.059	.89±.04	-	-	4.3 ±1.2	K	b)	.255
8-10	.048	.97±.02	-	-	5.6 ±1.1	π	b)	.269
8-11	.030	.94±.02	-	-	6.1 ±1.8	K	b)	.184
8-26	.049	.97±.03	-	-	2.7 ± .5	π	b)	.132
8-28	.097	.86±.02	-	-	$2.0\ ^{+1.3}_{-1.0}$	p	b)	.210
8-29	.142	.91±.04	-	-	$1.9\ ^{+1.2}_{-\ .9}$	π	b)	.268
9-1	.139	1.32±.05	20	1.72±.06	.72± .03	p	a)	.101
12-1	3.96	1.68±.06	9.3	2.45±.07	.47± .01	p	a)	.729
12-3	.183	.92±.03	-	-	2.2 ± .7	π	b)	.397
12-19	.23	.84±.02	-	-	.78± .21	π	b)	.178
12-22	.21	.93±.02	-	-	2.4 ± .4	π	b)	.494
13-1	.205	.94±.02	26	1.16±.03	2.1 ± .4	p	a),b)	.456
13-26	.115	.86±.02	-	-	3.5 ± .6	K	b)	.404
13-29	.20	.96±.02	-	-	3.3 ±1.0	π	[illegible]	
13-31	.175	[illegible]						
41-2	.966	2.47±.07	3.3	3.2 ±.14	.295±.002	p	a)	.395
41-14	.324	1.59±.05	-	-	.35± .14	K	b)	.152
41-15	.866	1.13±.04	21	1.67±.06	.51± .01	K	a)	.421
46-4	.320	.95±.03	-	-	2.6 ± .6	π	b)	.794
46-5	.283	.90±.03	-	-	4.3 ±1.2	K	b)	1.18
46-9	.210	.98±.02	-	-	3.9 ± .3	π	b)	.802

TABLE VIII

(continued)

Track[a] No.	tan θ_i	g_1^*	ΔR(cm)	g_2^*	$p\beta$	Iden-tity	Method used	p_t
46-36	.61	.86±.02	-	-	.55± .13	π	b)	.295
46-37	.75	.95±.03	6.6	.97±.04	.24± .02	π	a)	.162
47-1	.250	.82±.03	-	-	.76± .21	π	b)	.187
47-2	.066	.94±.02	-	-	$2.1 \begin{smallmatrix}+.8\\-.6\end{smallmatrix}$	π	b)	.139
47-3	.040	.98±.03	-	-	10.6 ±3.6	π	b)	.424
47-12	.152	.86±.03	4	.96±.03	.27± .02	π	a)	.045
47-13	.200	.87±.03	5.3	.96±.04	.25± .04	π	a)	.055
47-14	-3.08	.90±.03	3.9	.94±.04	.24± .04	π	a)	.257
49-2	.166	.93±.04	-	-	$3.7 \begin{smallmatrix}+1.5\\-1.2\end{smallmatrix}$	π	b)	.606
49-4	.022	.98±.03	-	-	8.4 ±2.4	π	b)	.185
49-7	.063	1.00±.03	-	-	$5.4 \begin{smallmatrix}+2.5\\-2.0\end{smallmatrix}$	π	b)	.340
59-1	.251	.88±.02	-	-	1.5 ± .3	π	b)	.367
59-2	.118	.89±.03	60.1	1.01±.03	1.77± .14	p	a)	.230
59-4	.084	.92±.03	-	-	1.1 ± .3	K	b)	.100
59-15	.044	.97±.04	-	-	$2.5 \begin{smallmatrix}+1.0\\-.8\end{smallmatrix}$	π	b)	.110
59-58	.165	.96±.03	-	-	3.2 ± .9	π	b)	.521
59-64	.040	.99±.03	-	-	$3.5 \begin{smallmatrix}+1.4\\-1.2\end{smallmatrix}$	π	b)	.140
72-G1	1.264	3.2 ±.1	-	-	.28± .07	p	b)	.433
72-36	.308	.90±.02	-	-	1.2 ± .2	K	b)	.378
72-37	.405	.94±.02	-	-	1.8 ± .3	π	b)	.678
72-38	25.6	1.24±.05	4.8	1.44±.05	.40± .02	K	a)	.541
77-2	.225	.89±.03	-	-	1.9 ± .4	π	b)	.418
77-3	.21	.87±.03	-	-	$1.3 \begin{smallmatrix}+.8\\-.5\end{smallmatrix}$	π	b)	.269
77-4	.13	.97±.04	-	-	3.4 ± .7	π	b)	.439

TABLE VIII

(continued)

Track[a] No.	tan θ_i	g_1^*	ΔR(cm)	g_2^*	$p\beta$	Identity	Method used	p_t
77-5	.114	.92±.03	-	-	$1.9^{+.9}_{-.7}$	π	b)	.216
77-7	.096	.92±.03	-	-	4.8 ±1.1	π	b)	.459
77-8	.088	.92±.03	-	-	6.4 ±1.8	K	b)	.563
77-14	.014	.95±.03	-	-	5.5 ±1.4	π	b)	.077
77-26	.049	.93±.03	-	-	11.1 ±3.1	K	b)	.544
77-27	.044	.98±.04	-	-	$14.6^{+15.5}_{-11.7}$	π	b)	.642
77-33	.328	.85±.02	-	-	.85± .18	π	b)	.268
109-1	.175	.90±.02	40	1.10±.02	.90± .04	K	a)	.173
109-7	.172	.99±.04	43	1.08±.03	1.36± .08	p	a)	.268
116-4	.028	.91±.03	-	-	5.5 ±1.1	K	b)	.155
116-6	.014	.97±.03	-	-	4.9 ±1.1	π	b)	.069
116-7	.080	.97±.02	-	-	6.3 ±1.4	π	b)	.503
116-8	.14	.88±.03	-	-	$1.5^{+.6}_{-.5}$	π	b)	.209
117-4	.100	.89±.03	-	-	$1.6^{+.8}_{-.6}$	π	b)	.160
117-6	.105	.94±.02	-	-	1.8 ± .6	π	b)	.189
117-16	.186	1.00±.03	-	-	$3.3^{+2.2}_{-1.6}$	π	b)	.604
118-1	.13	.96±.01	-	-	2.2 ± .7	π	b)	.284
118-2	.143	1.07±.04	-	-	.38± .10	K	b)	.074
118-3	.095	1.10±.05	-	-	$.11^{+.05}_{-.04}$	π	b)	.014
118-4	.085	.94±.04	-	-	$4.7^{+2.6}_{-2.0}$	π	b)	.398
118-5	.044	.99±.04	-	-	4.7 ±1.5	π	b)	.207
118-18	.010	1.00±.04	-	-	6.7 ±1.8	π	b)	.067

TABLE VIII

(continued)

Track No.[a]	tan θ_i	g_1^*	ΔR(cm)	g_2^*	$p\beta$	Iden-tity	Method used	p_t
118-19	.023	.94±.03	-	-	$2.0\ ^{+1.1}_{-.9}$	π	b)	.046
118-20	.047	1.04±.05	-	-	7.3 ±2.8	π	b)	.343
120-1	.422	.99±.02	-	-	2.9 ± .5	Y	b)	1.27

[a]The number before a dash is the event number, and that after the dash is the secondary's number.

LIST OF ILLUSTRATIONS

LIST OF ILLUSTRATIONS

(continued)

LI OF ILLUSTRATI

(continued)

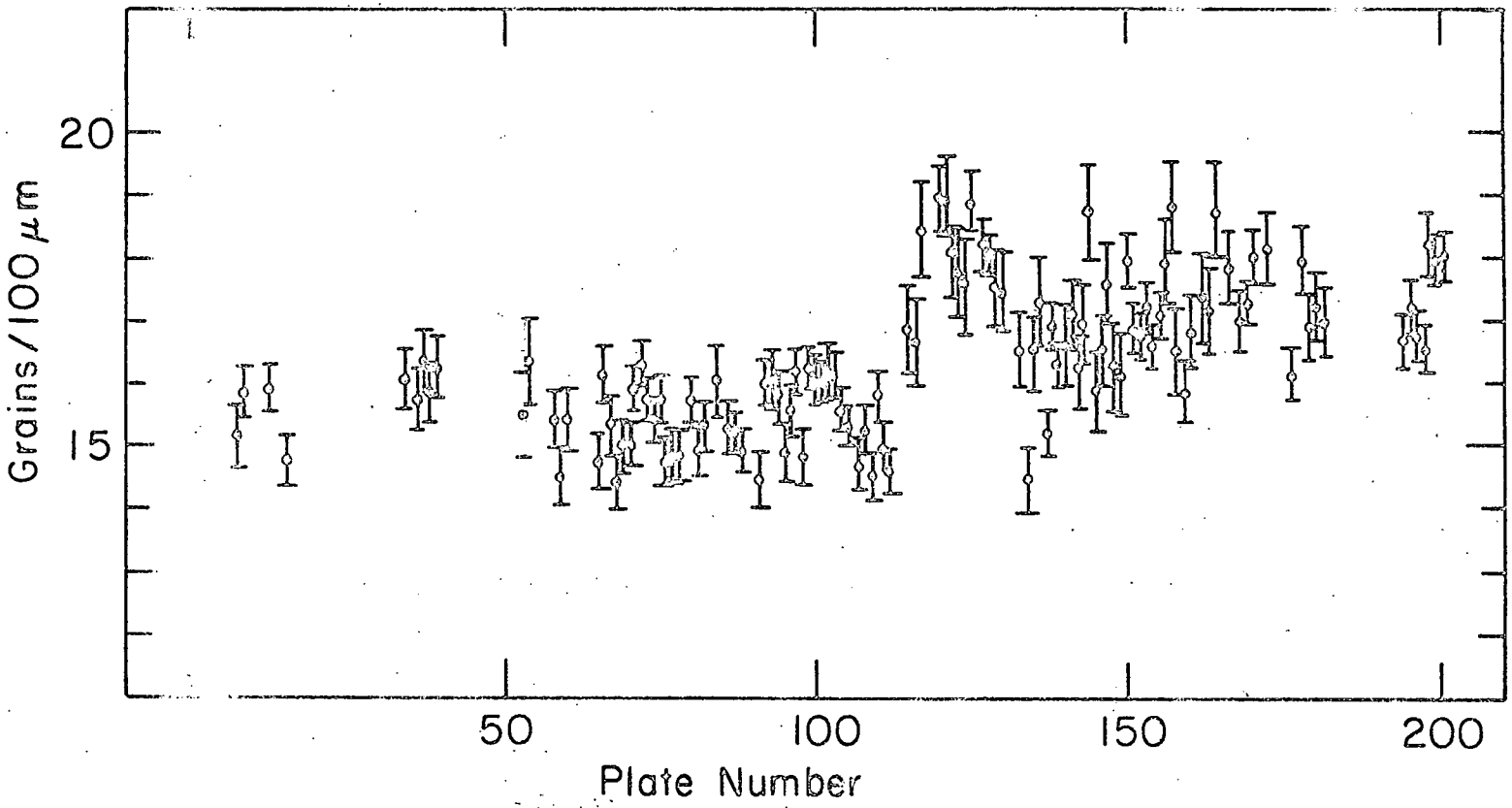

Fig. 1

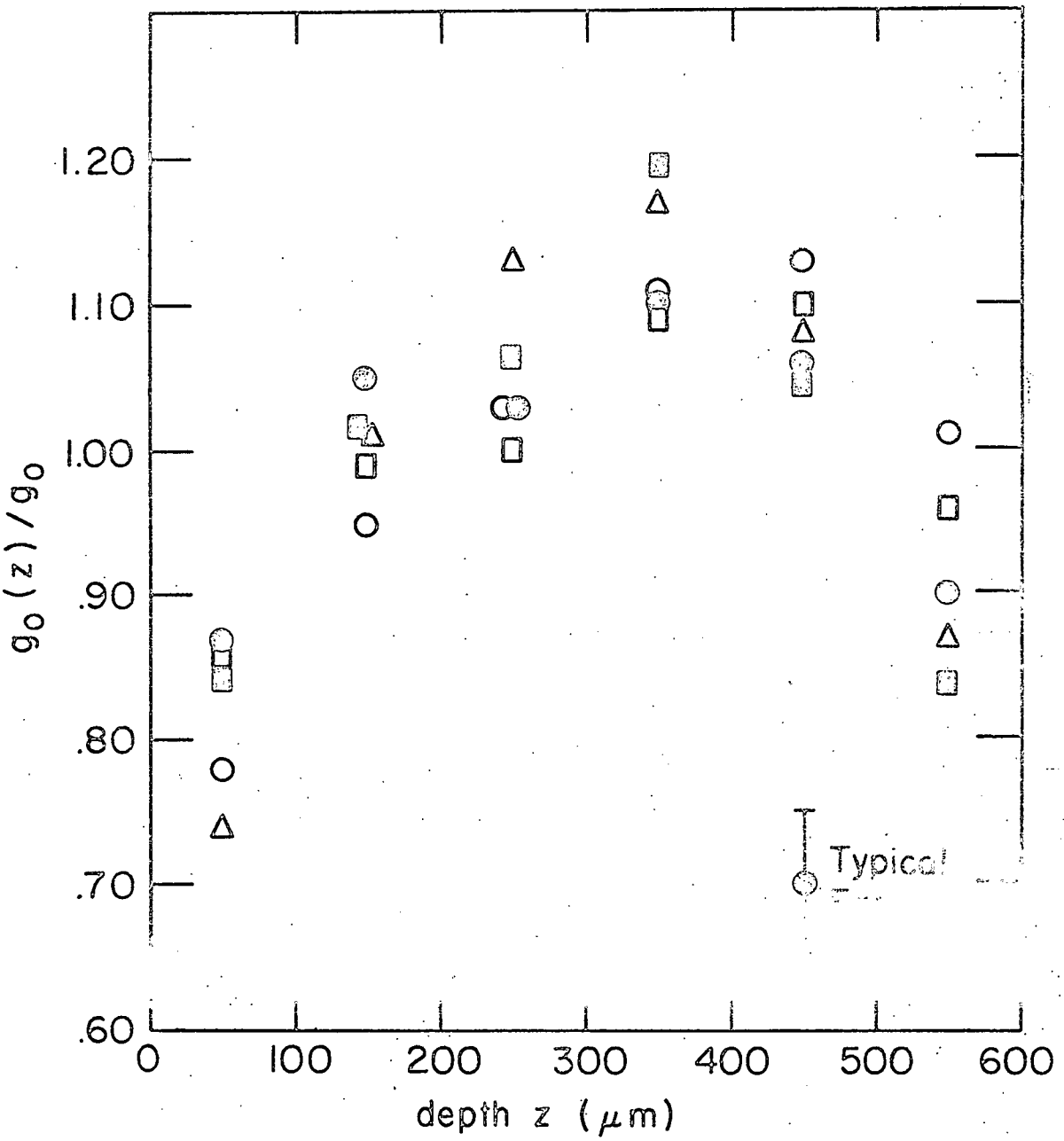
1.20
1.10
1.00
.90
.80
.70
.60
$g_o(z)/g_o$
0
100
200
300
400
500
600
depth z (μm)
Typical

Fig. 2

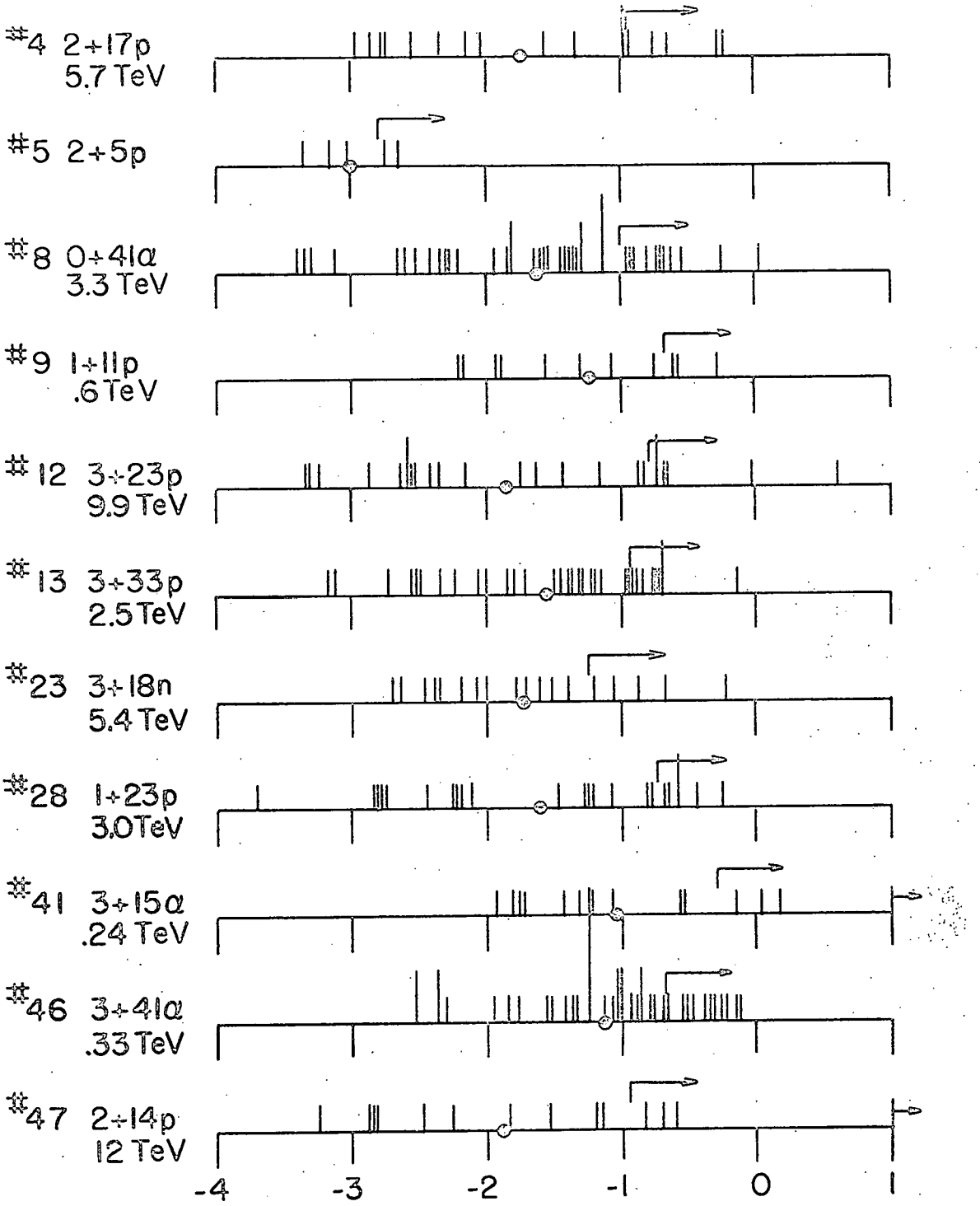
#4 2÷17p
5.7 TeV
#5 2÷5p
#8 0÷41α
3.3 TeV
#9 1÷11p
.6 TeV
#12 3÷23p
9.9 TeV
#13 3÷33p
2.5 TeV
#23 3÷18n
5.4 TeV
#28 1÷23p
3.0 TeV
#41 3÷15α
.24 TeV
#46 3÷41α
.33 TeV
#47 2÷14p
12 TeV
-4
-3
-2
-1
0
1

Fig.3(a)

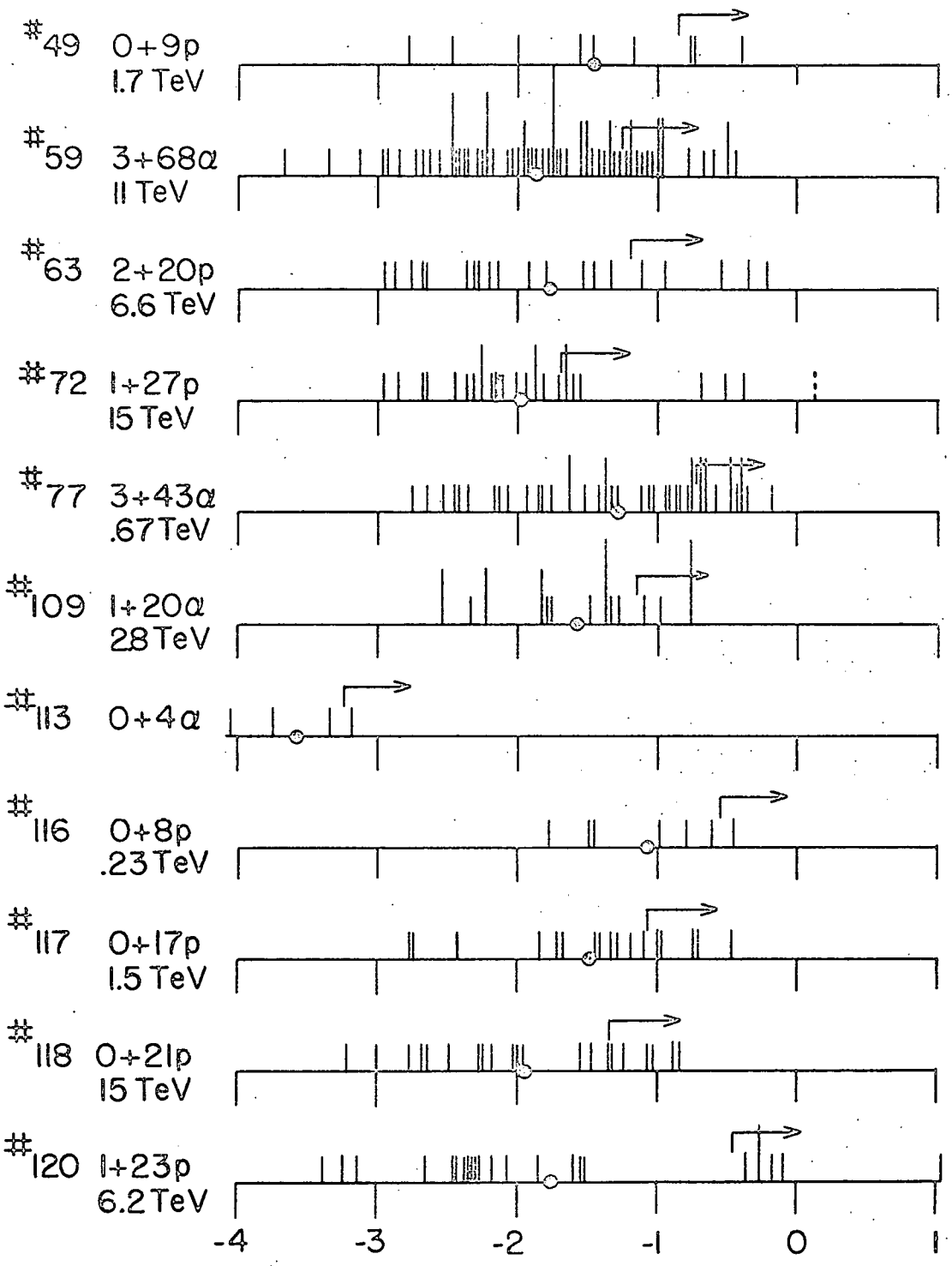
#49 0+9p 1.7 TeV
#59 3+68α 11 TeV
#63 2+20p 6.6 TeV
#72 1+27p 15 TeV
#77 3+43α .67 TeV
#109 1+20α 28 TeV
#113 0+4α
#116 0+8p .23 TeV
#117 0+17p 1.5 TeV
#118 0+21p 15 TeV
#120 1+23p 6.2 TeV
-4
-3
-2
-1
0
1

Fig. 3(b)

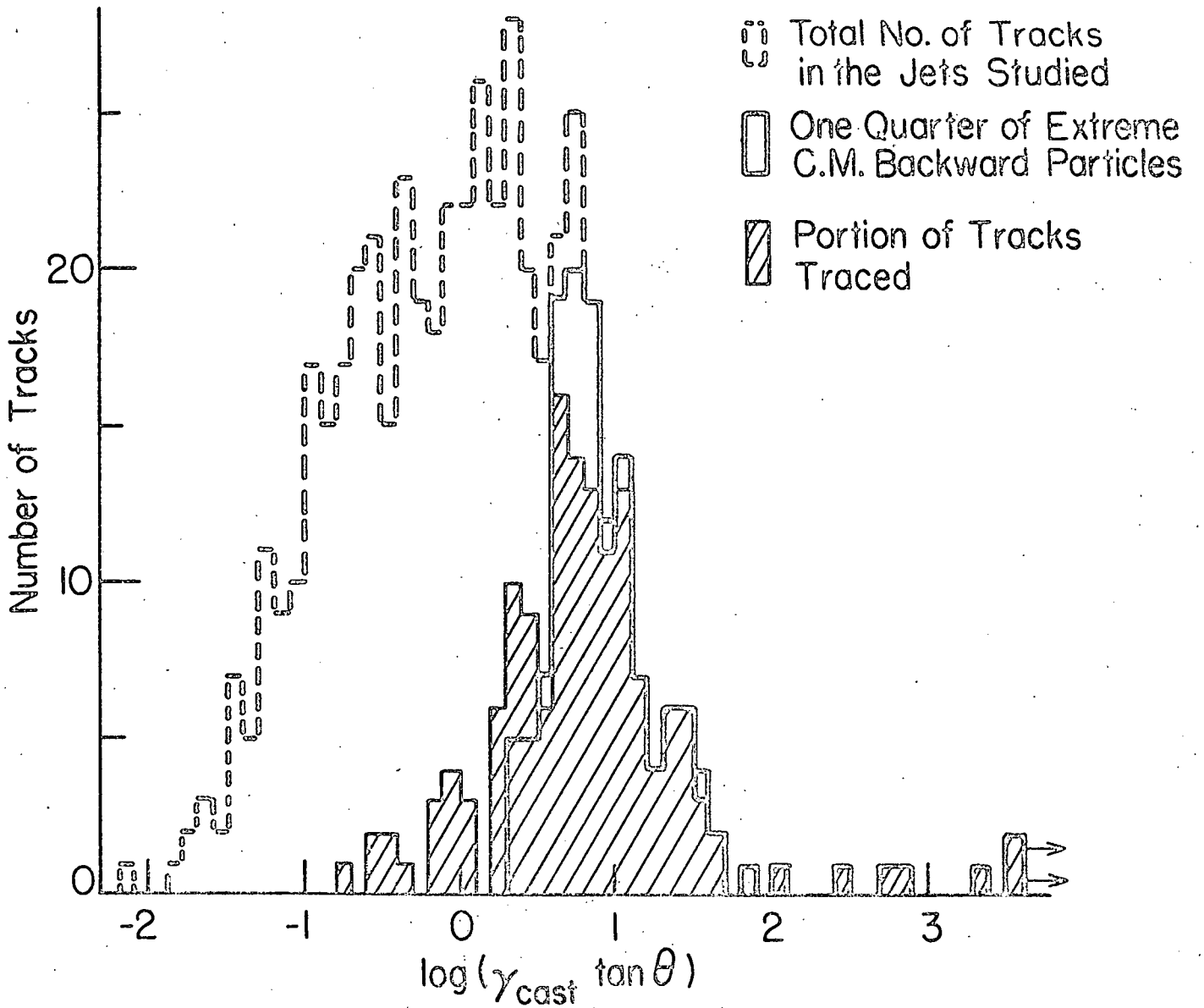
Total No. of Tracks in the Jets Studied
One Quarter of Extreme C.M. Backward Particles
Portion of Tracks Traced
Number of Tracks
0
10
20
-2
-1
0
1
2
3
log (γ_{cast} tan θ)

Fig.4

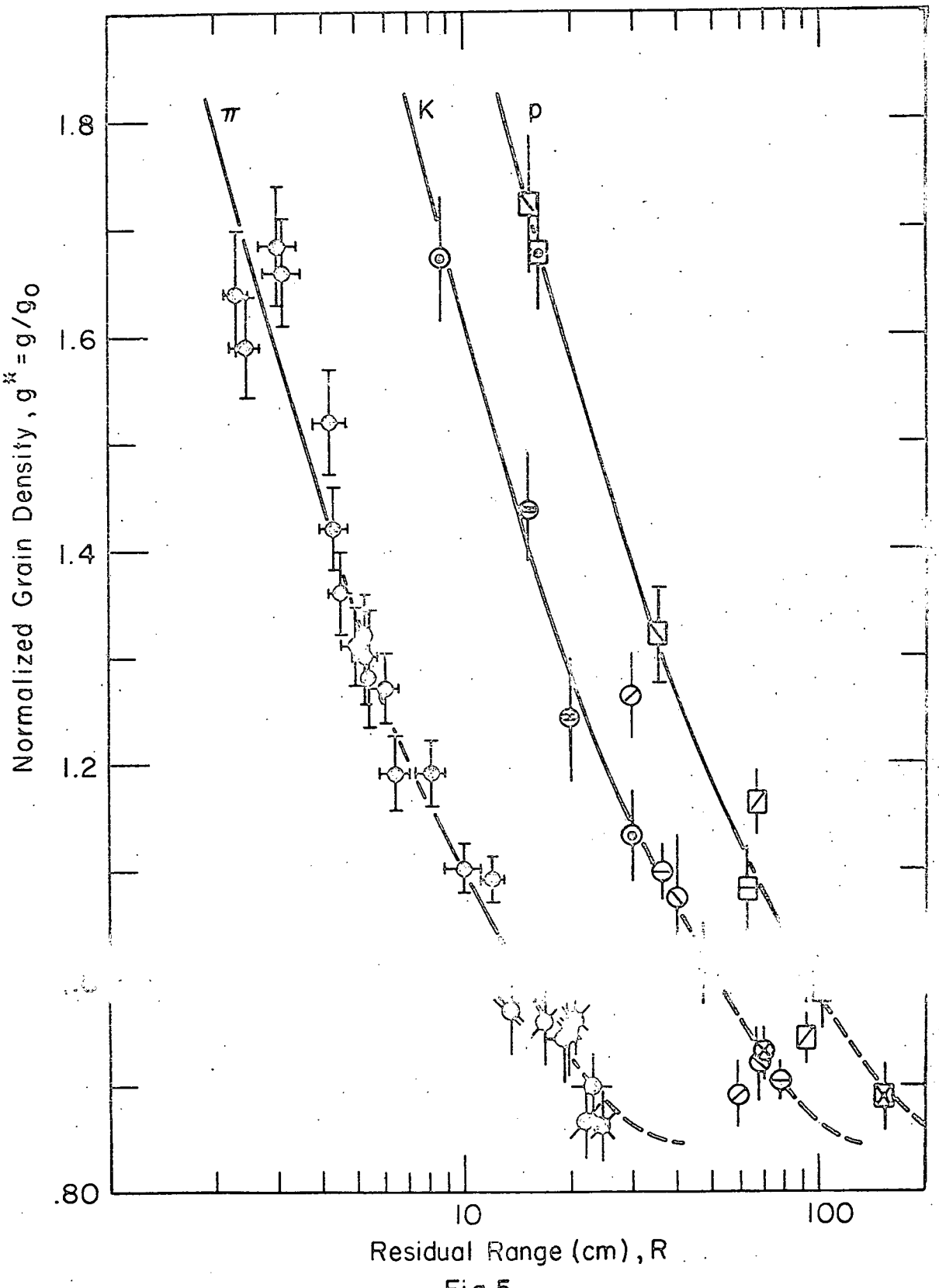
π
K
p
1.8
1.6
1.4
1.2
.80
Normalized Grain Density, $g^* = g/g_o$
10
100
Residual Range (cm), R

Fig.5

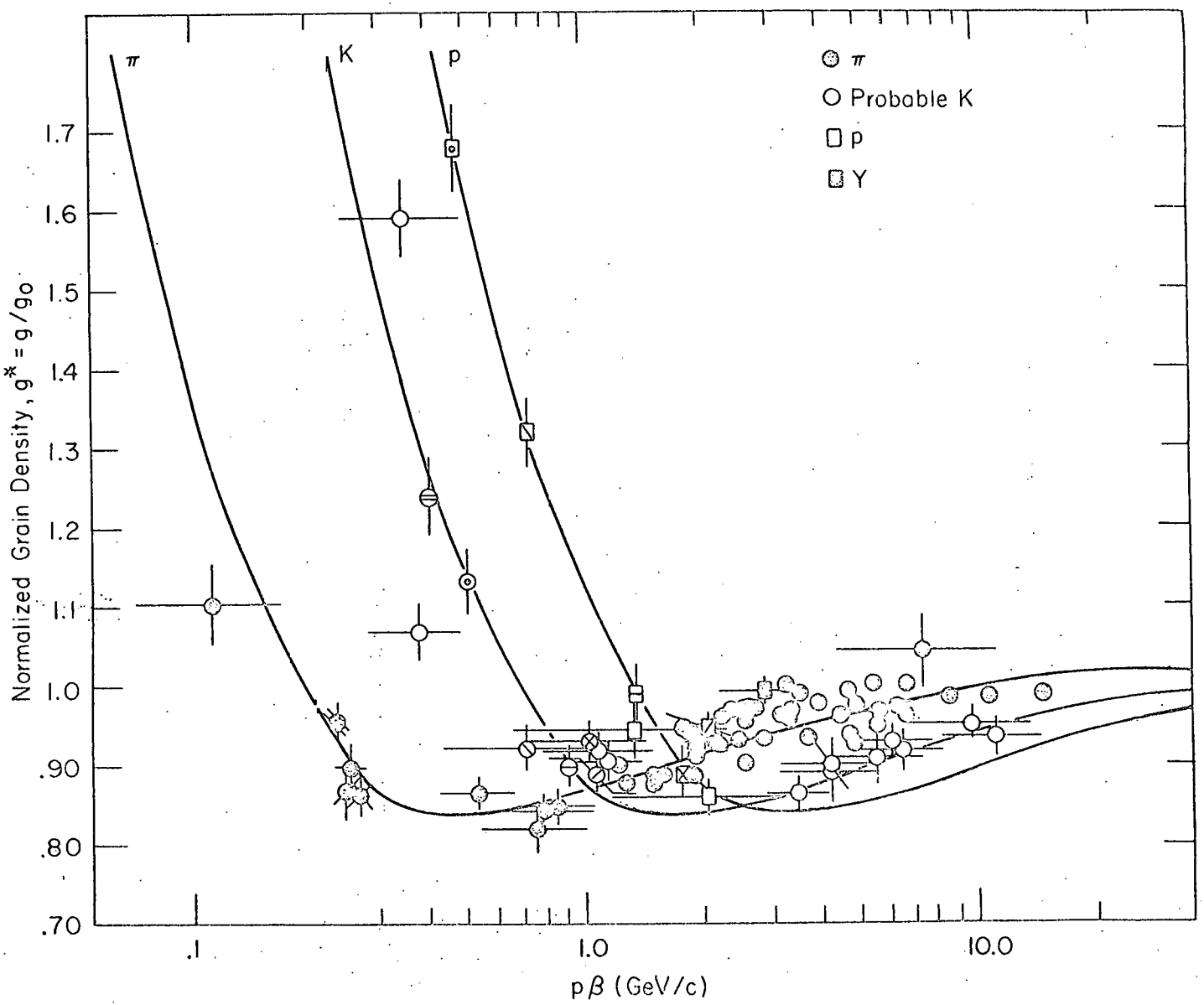
π
K
p
π
Probable K
p
Y
Normalized Grain Density, g* = g/g0
1.7
1.6
1.5
1.4
1.3
1.2
1.1
1.0
.90
.80
.70
.1
1.0
10.0
pβ (GeV/c)

Fig.6

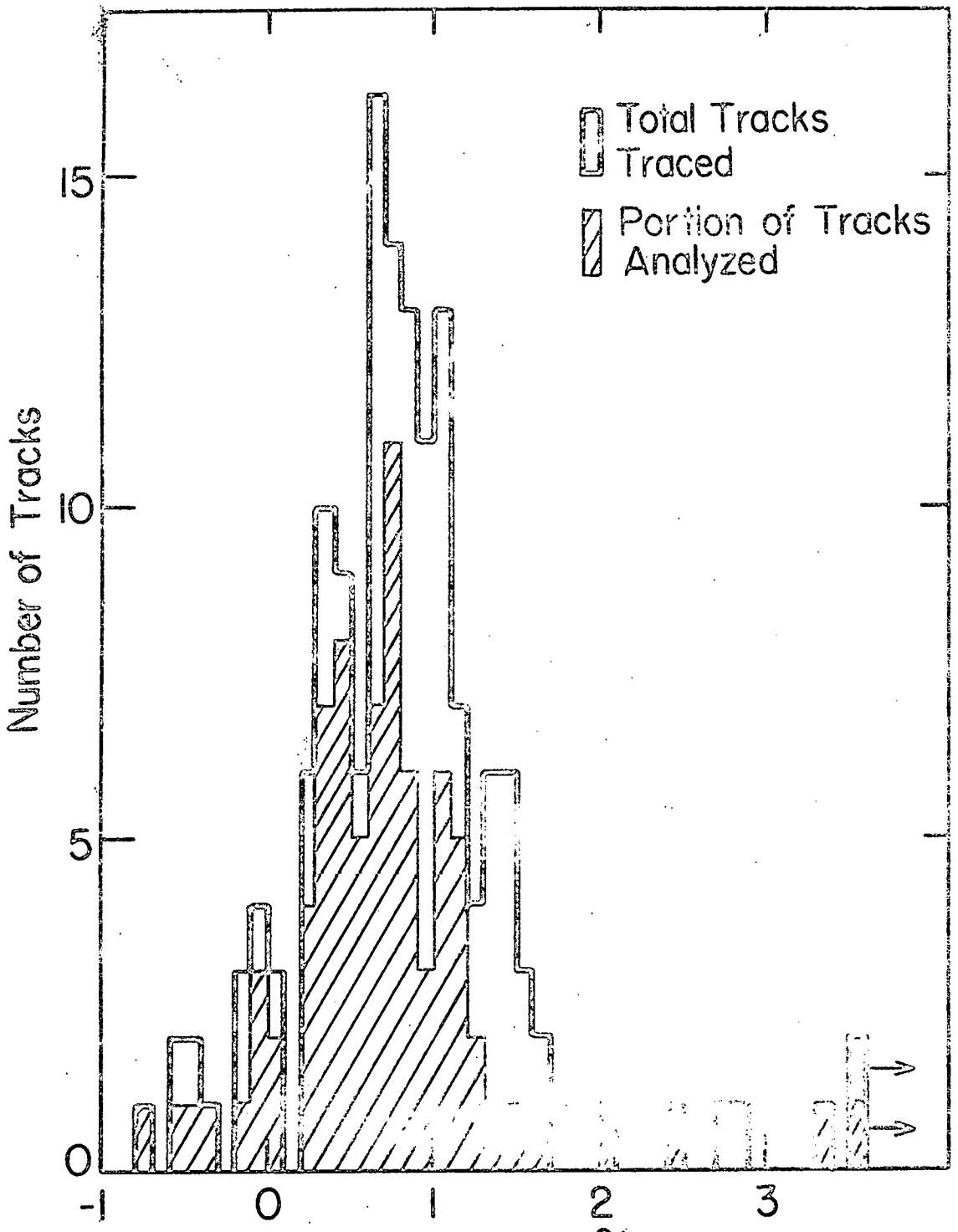
Total Tracks Traced
Portion of Tracks Analyzed
Number of Tracks
0
5
10
15
-1
0
1
2
3
log(γcast tan θ)

Fig.7(a)

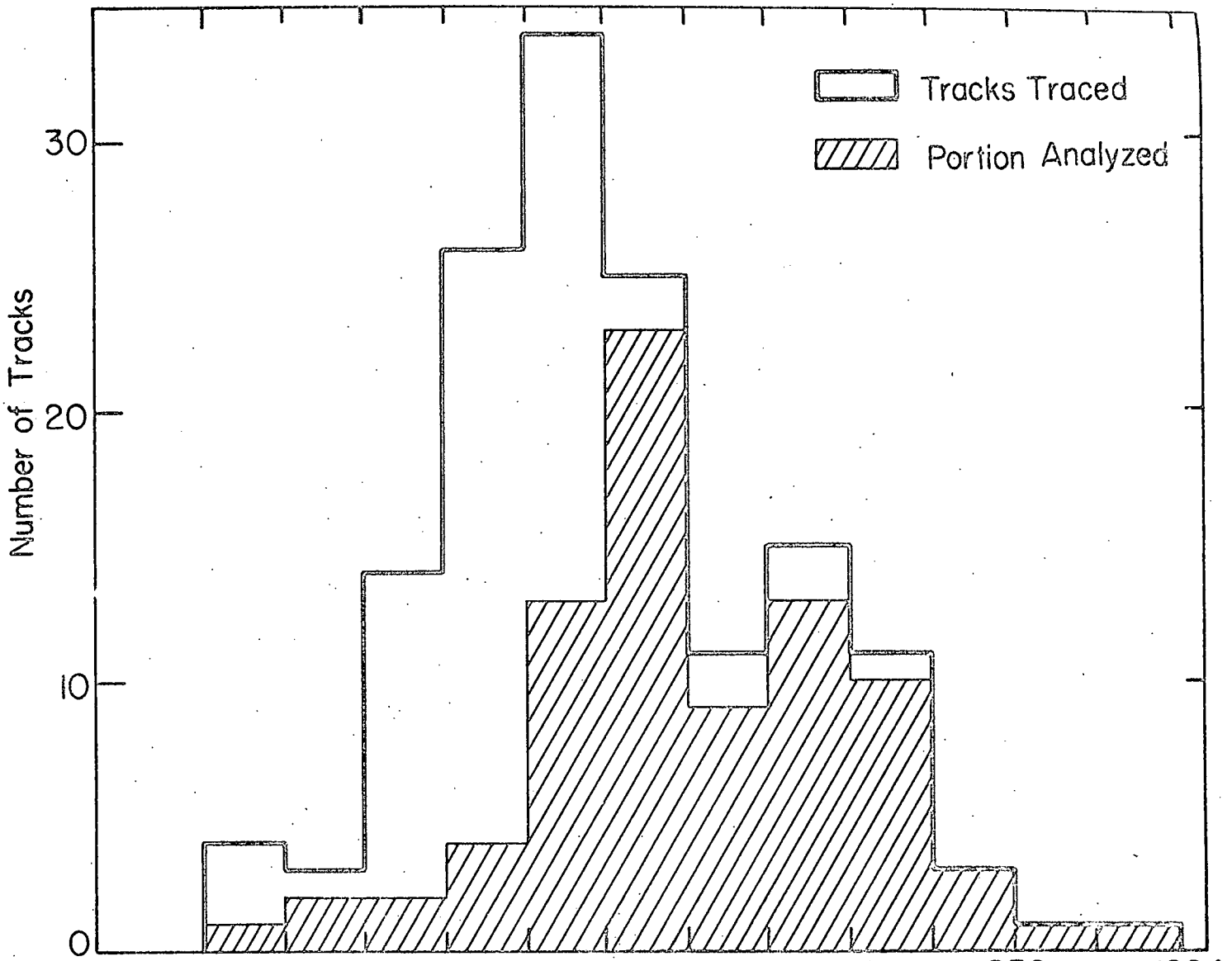
Tracks Traced
Portion Analyzed
Number of Tracks
0
10
20
30
.25
1
4
16
64
256
1024
Track Length per Plate (mm)

Fig. 7(b)

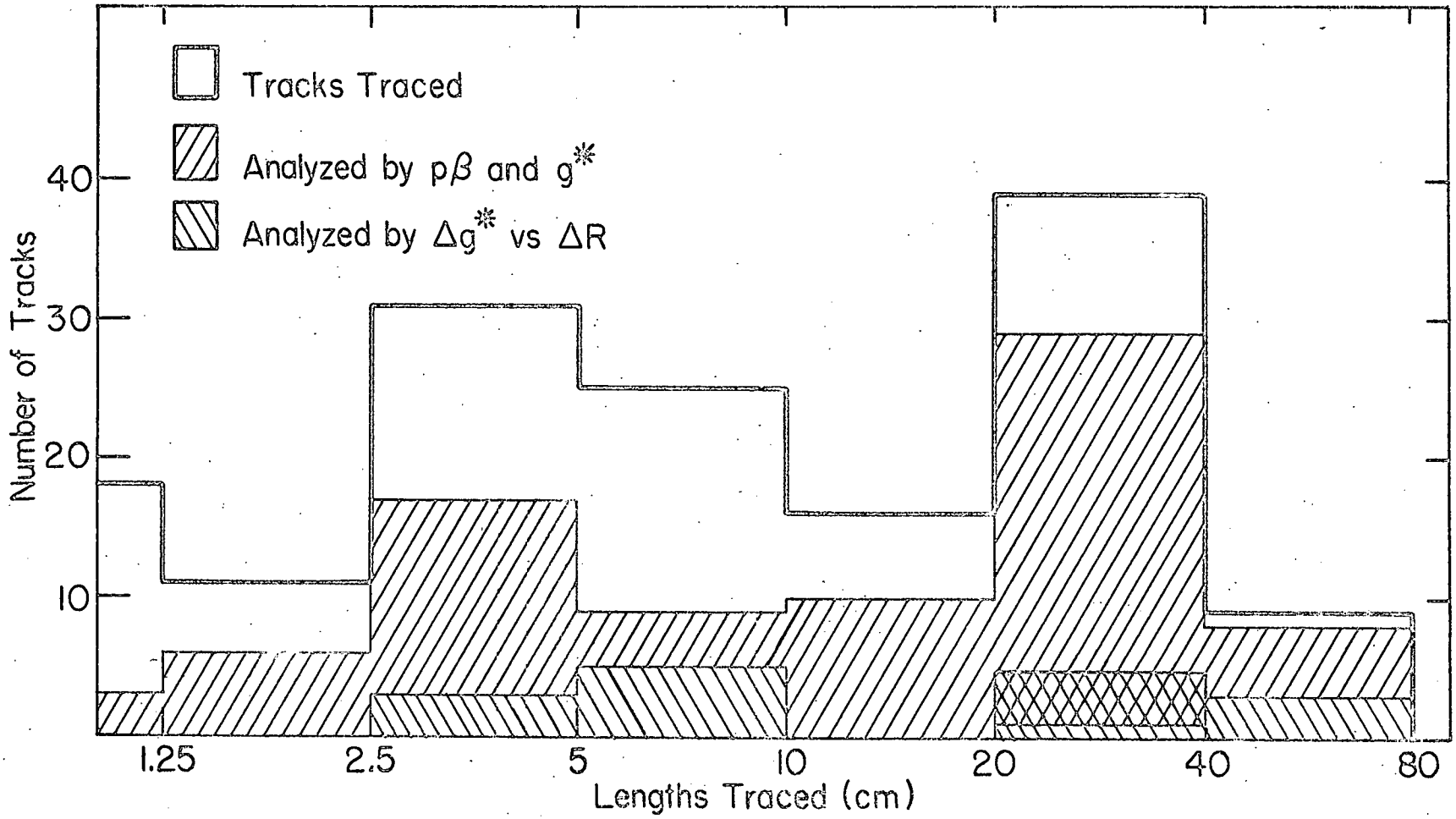
Tracks Traced
Analyzed by pβ and g*
Analyzed by Δg* vs ΔR
Number of Tracks
40
30
20
10
1.25
2.5
5
10
20
40
80
Lengths Traced (cm)

Fig. 7(c)

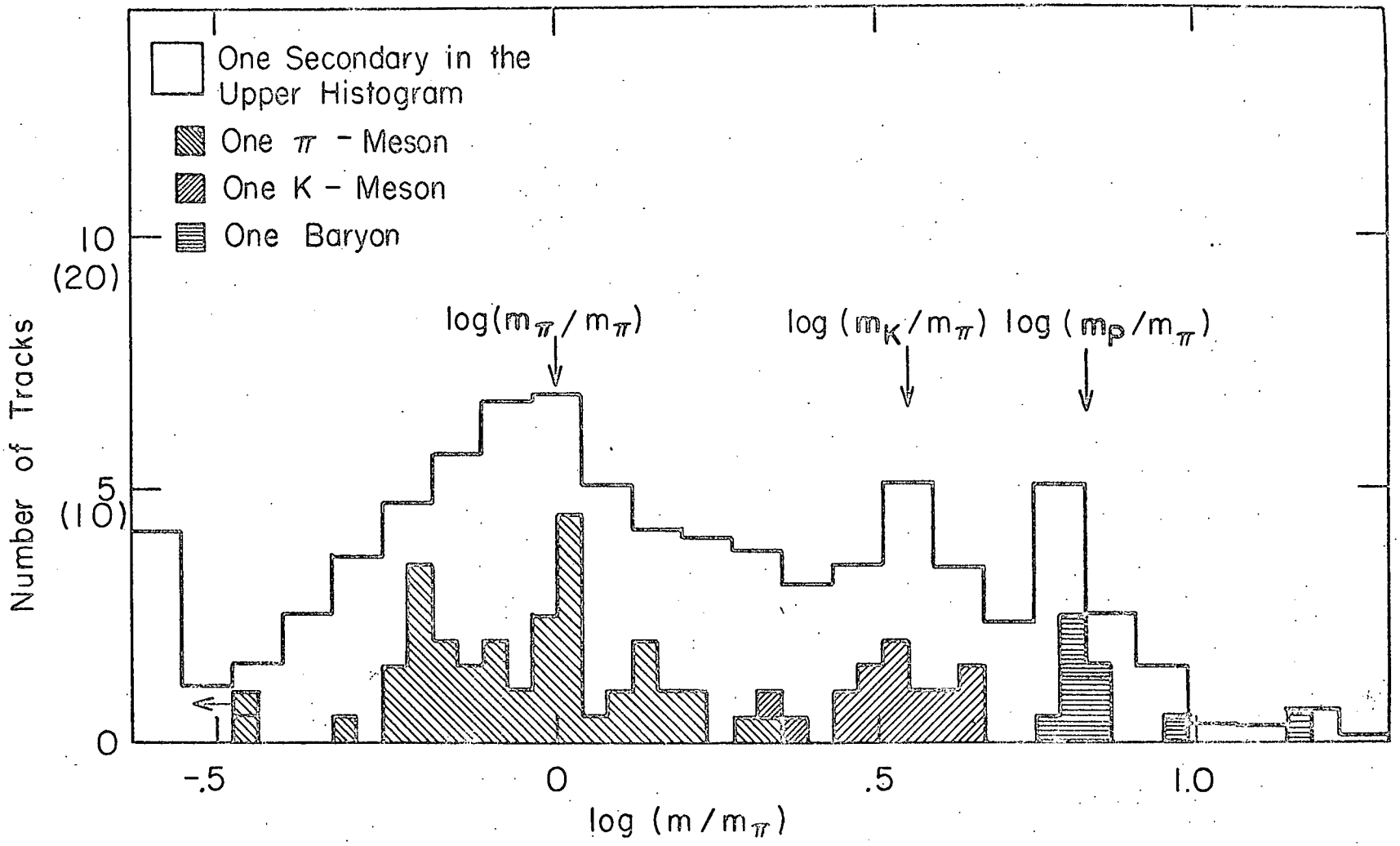
One Secondary in the Upper Histogram
One π - Meson
One K - Meson
One Baryon
10
(20)
5
(10)
0
Number of Tracks
log(m_π / m_π)
log (m_K / m_π)
log (m_p / m_π)
-.5
0
.5
1.0
log (m / m_π)

Fig. 8

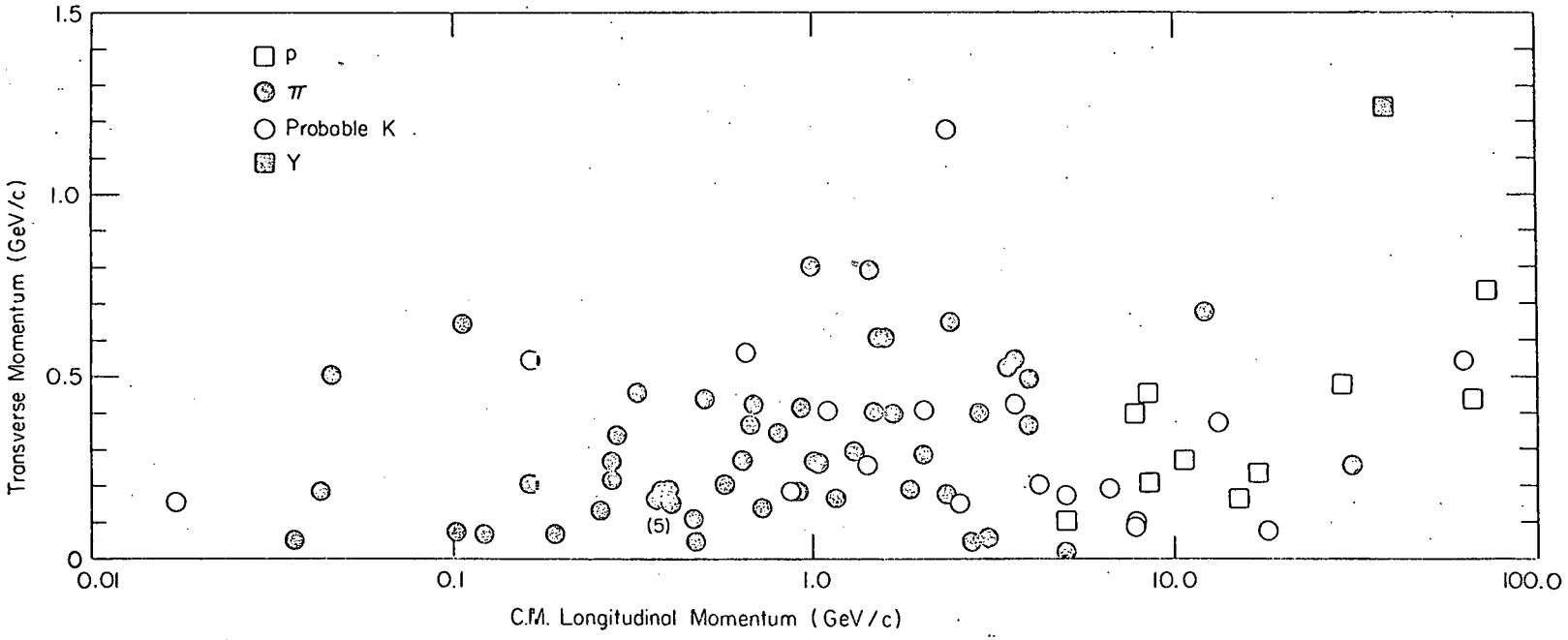
p
π
Probable K
Y
(5)
Transverse Momentum (GeV/c)
C.M. Longitudinal Momentum (GeV/c)
0
0.5
1.0
1.5
0.01
0.1
1.0
10.0
100.0

Fig. 9

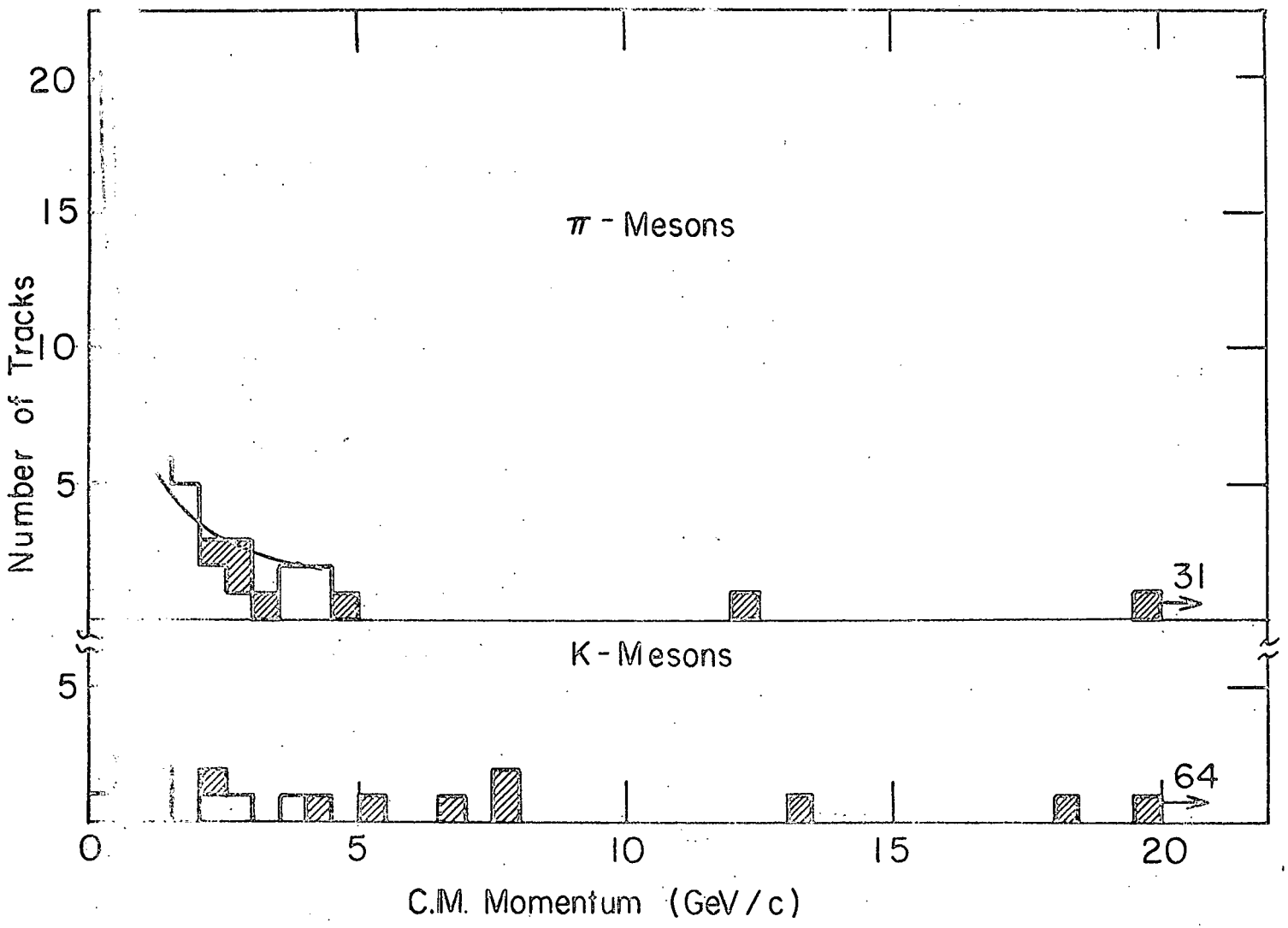
20
15
10
5
5
Number of Tracks
π - Mesons
31
K - Mesons
64
0
5
10
15
20
C.M. Momentum (GeV/c)

Fig. 10

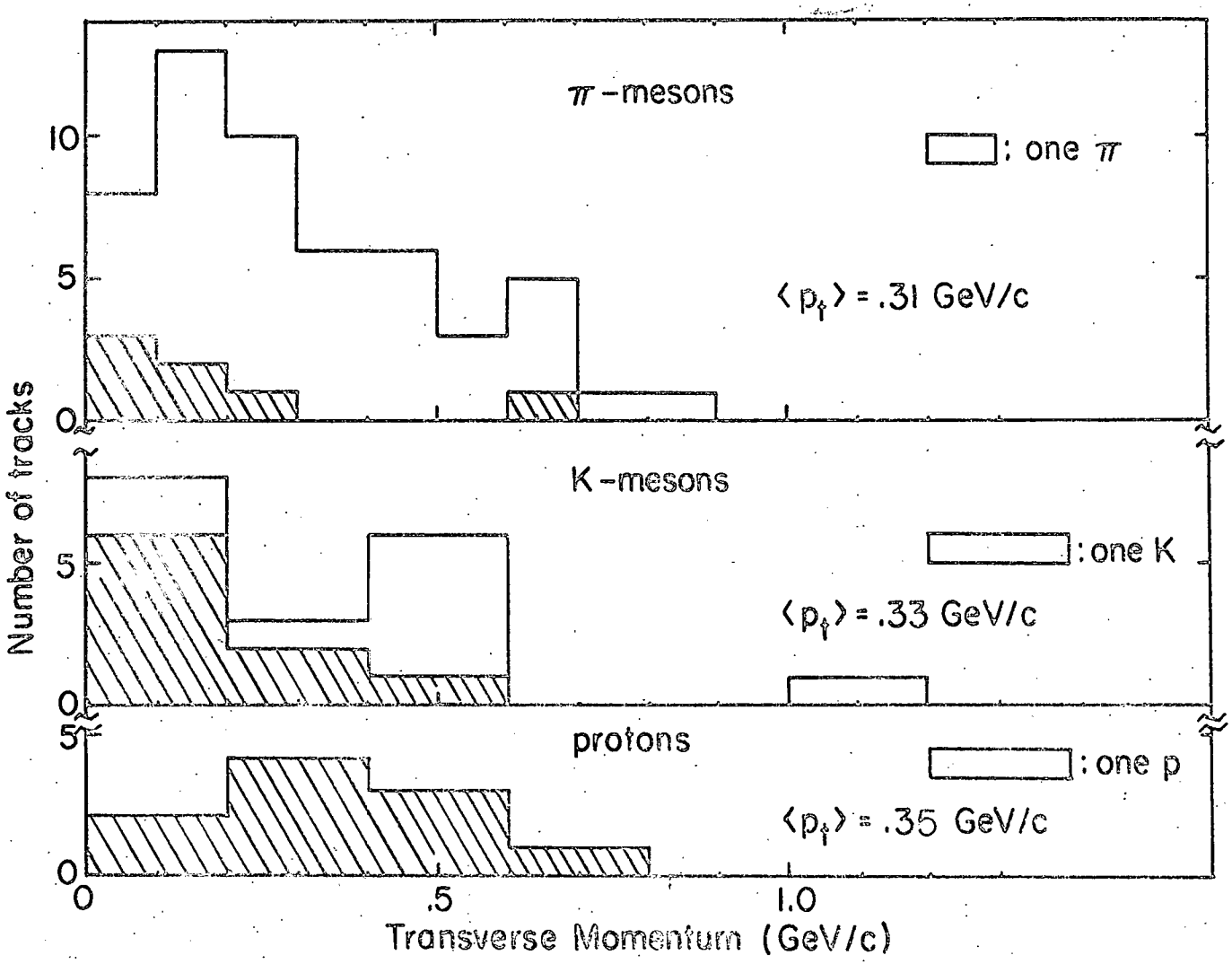
π -mesons
: one π
⟨ p_t ⟩ = .31 GeV/c
K -mesons
: one K
⟨ p_t ⟩ = .33 GeV/c
protons
: one p
⟨ p_t ⟩ = .35 GeV/c
Number of tracks
10
5
0
5
0
5
0
0
.5
1.0
Transverse Momentum (GeV/c)

Fig. 11

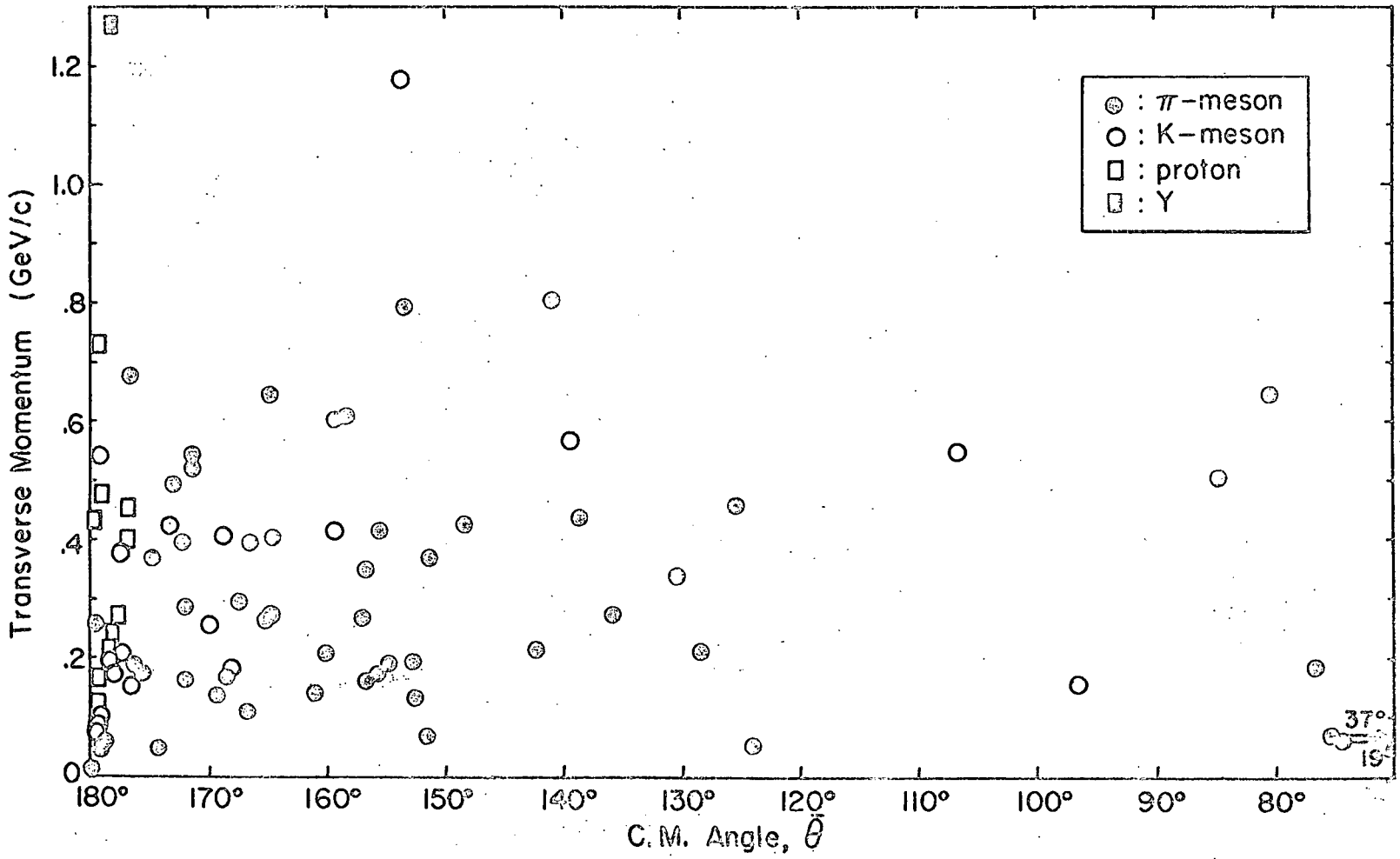
Transverse Momentum (GeV/c)
1.2
1.0
.8
.6
.4
.2
0
180°
170°
160°
150°
140°
130°
120°
110°
100°
90°
80°
C.M. Angle, θ
: π−meson
: K−meson
: proton
: Y
37°
19°

Fig. 12

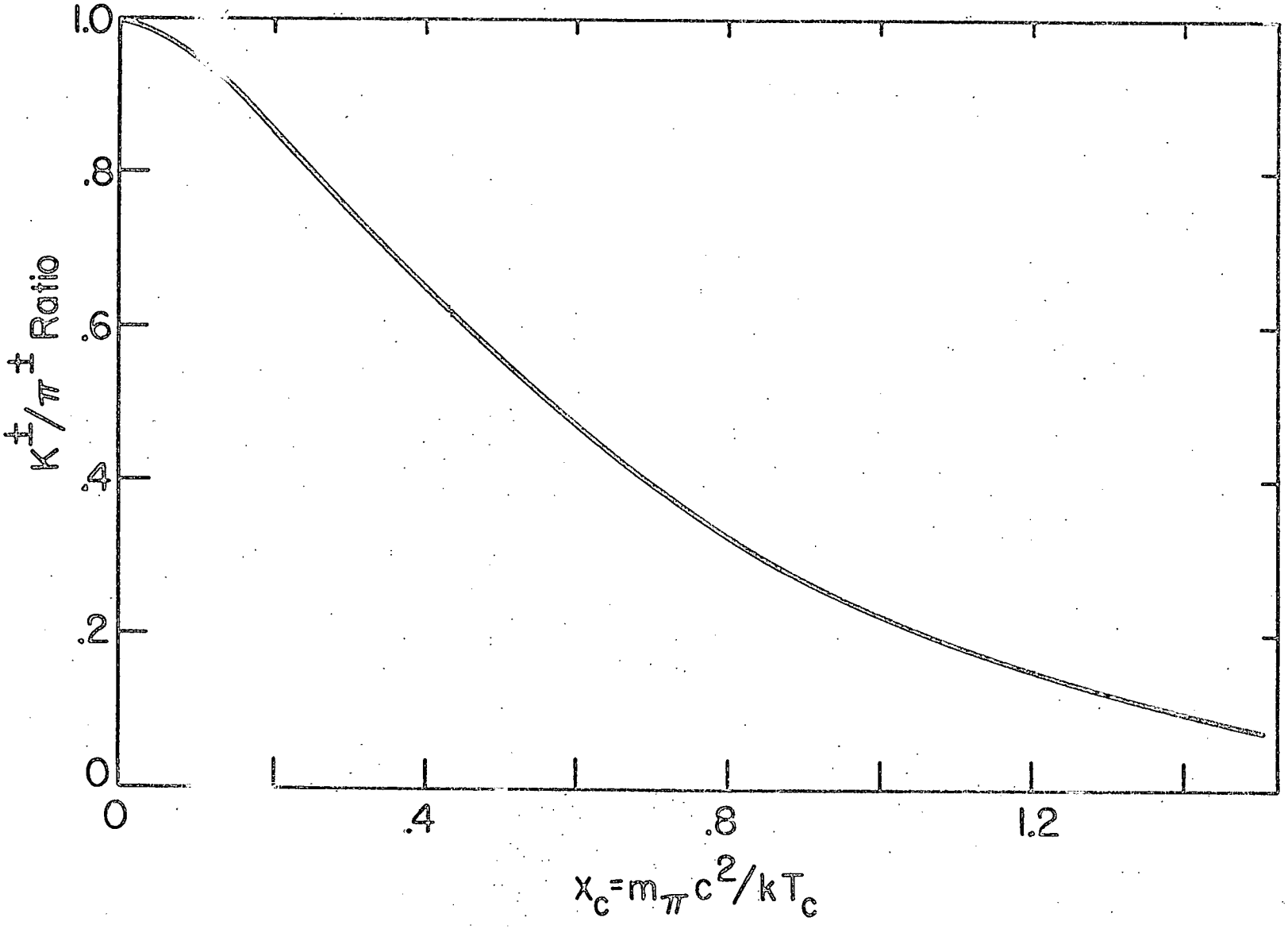

Fig.13

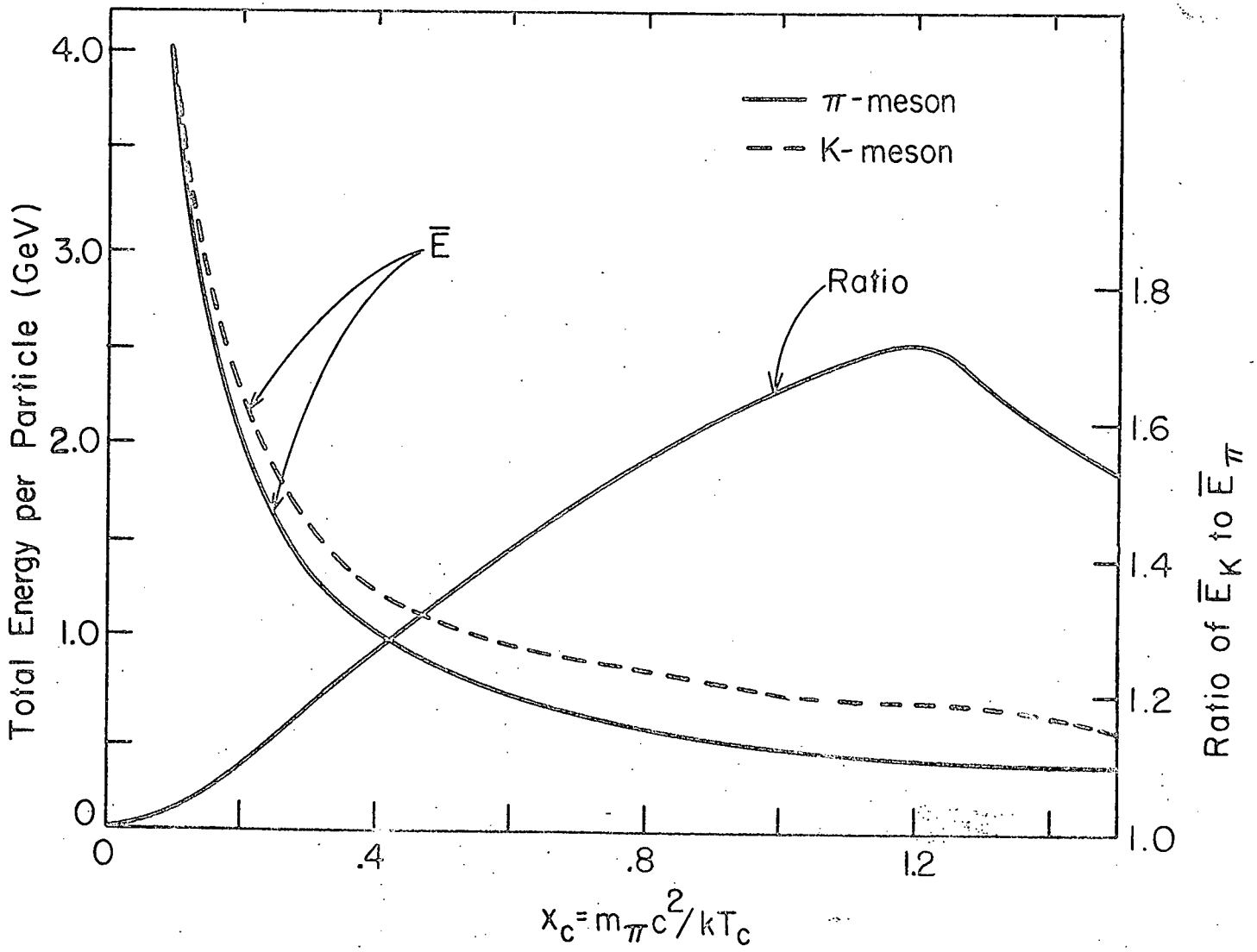
π-meson
K-meson
$\bar{E}$
Ratio
Total Energy per Particle (GeV)
Ratio of $\bar{E}_K$ to $\bar{E}_\pi$
4.0
3.0
2.0
1.0
0
1.8
1.6
1.4
1.2
1.0
0
.4
.8
1.2
$x_c = m_\pi c^2 / kT_c$

Fig.14

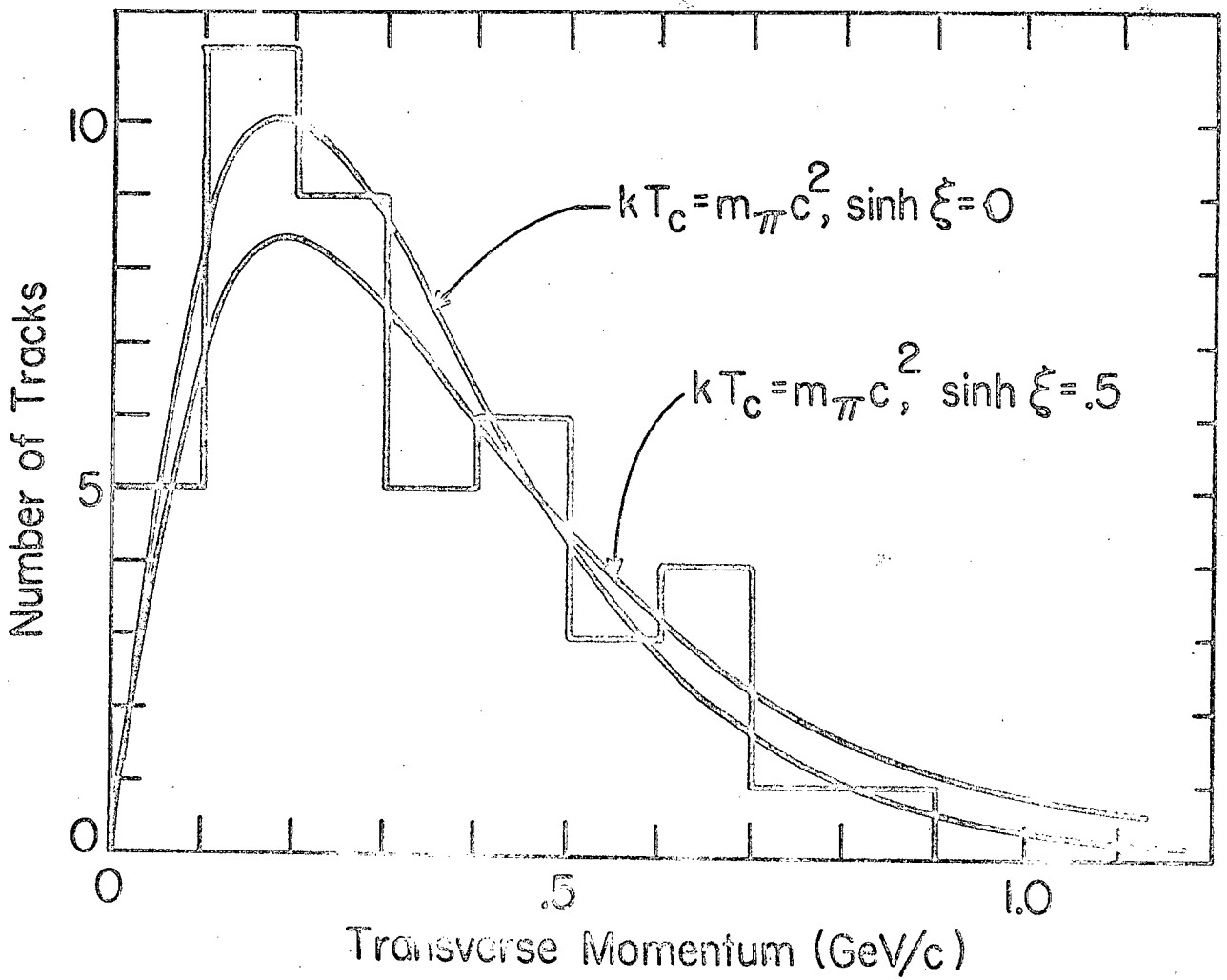
10
5
0
0
.5
1.0
Number of Tracks
Transverse Momentum (GeV/c)
$kT_c = m_\pi c^2$, sinh $\xi = 0$
$kT_c = m_\pi c^2$, sinh $\xi = .5$

Fig.15